Petrofacies of Eocene sand injectites of the Tumey Giant Injection Complex, California (USA)

G. Zvirtes[a,c*], R.P. Philipp[b], A. Hurst[a], G. Palladino[a,d], L.F. De Ros[b], A. Grippa[a]

[a] *Department of Geology and Petroleum Geology, University of Aberdeen, Aberdeen, AB24 3FX, United Kingdom.*

[b] *Department of Mineralogy and Petrology, Federal University of Rio Grande do Sul, Porto Alegre, AV. Bento Gonçalves, 9500, RS, Brazil.*

[c] *Programa de Pós-graduação em Geociências (PPGGEO), Federal University of Rio Grande do Sul, Porto Alegre, AV. Bento Gonçalves, 9500, RS, Brazil.*

[d]*Dipartimento di Scienze, Università degli Studi della Basilicata, Potenza, Italy*

**Corresponding author (e-mail: g.zvirtes@abdn.ac.uk)*

Abstract

The forearc succession of Great Valley Group in Central California provides some of the best examples of giant sand injection complexes in the world and is therefore considered valuable analogues for injectite systems in subsurface. Several sand injection complexes are well described in the outcrop and subsurface, however the petrographic characteristics of injectites are still poorly documented. In this paper, we present the results of an integrated study of field observations, quantitative and qualitative sandstone petrography, provenance, and petrofacies analysis of the Tumey Giant Injection Complex (TGIC) in order to understand its lithostratigraphy and petrological evolution, and its impacts on reservoir petrofacies characteristics and fluid migration. The TGIC intrudes into a 450 m thick deep-water succession of slope mudrocks and sandy channel-fills of the Kreyenhagen Shale Eocene), forming an interconnected network of sandstone sills, dykes and injection breccias. The complex generated a horizontal and vertical plumbing system for fluid migration, connecting isolated sandy channel-fills among low-permeability mudrocks. The primary detrital composition, diagenetic products, microtextures, and provenance signatures allowed for the definition and discrimination of depositional and intrusive petrofacies and their genetic relations. Petrofacies associations confirm that the gypsum-cemented feldspathic litharenites from the Kreyenhagen Shale channel-fills are the only source for the injection complex. Eodiagenetic compaction and extensive gypsum cementation reduced the primary porosity of the complex, while telodiagenetic dissolution of autigenic constituents formed pervasive secondary porosity. The underlying calcite-cemented arkosic sandstones of the Lodo and Domengine formations acted as barriers for fluid flow, aiding lateral fluid migration and overpressure buildup within the overlying Kreyenhagen channel-fills. Intense grain microfracturing occurred during sand remobilization and injection along with erosion of the host mudrocks. This study has significance for the generation of reliable stratigraphic and petrological models for sand injection complex genesis and evolution that consequently can help the understanding and exploration of injectite complexes elsewhere.

Keywords: Sand injection complex; Sandstone petrography; Injectite Provenance; Reservoir petrofacies; Intragranular microfracturing; Fluid flow

1. Introduction

Sand injectites form when fluidized sand is ‘forcedly’ emplaced into low-permeability host strata, creating a network of dikes, sills, pipes, injection breccias and other irregular intrusions. They are described from many depositional settings (Jolly and Lonergan, 2002) but are commonly recorded in deep-marine environments associated with submarine fans and turbiditic successions (Hiscott 1979; Archer 1984; Vigorito et al., 2008; Hurst et al., 2015). In deep-water settings, sandy channel-fills are sealed by shales and other low-permeable strata, trapping pressurized fluids during increasing burial and compaction (Cartwright et al., 2007). Eventually, when pore-fluid overpressure inside the channel-fills reach the lithostatic pressure of the surrounding rocks, hydraulic fractures propagate into the host strata, triggering sand fluidization and injection, forming injectites (Jolly and Lonergan, 2002; Vigorito and Hurst, 2010).

Sand intrusions have been described for almost 200 years (e.g., Murchinson, 1827; Diller, 1890; Newsom, 1903; Hiscott, 1979; Surlyk and Noe-Nygaard, 2001; Palladino et al., 2018). For most of this time, they were considered localized geological oddities, without basin-scale influence. However, this view changed drastically after the recognition of injectites associated with hydrocarbon reservoirs (Dixon et al., 1995), particularly from their seismic interpretation (Huuse et al., 2007; Lonergan and Cartwright, 1999; MacLeod et al., 1999). During the past decades, numerous papers have emerged from the study of large-scale injectites in the subsurface (e.g., Dixon et al., 1995; Bergslien, 2002; Duranti and Hurst, 2004; Huuse et al., 2004; Schwab et al., 2015) and outcrops (e.g., Boehm and Moore, 2002; Schwartz et al., 2003; Surlyk et al., 2007; Vigorito et al., 2008; Scott et al., 2013; Palladino et al., 2016, 2018; Zvirtes et al., 2019). In terms of hydrocarbon exploration, large scale injection complexes (extending hundreds of meters vertically and several kilometres laterally) form vertical and lateral communication between reservoirs separated by low permeability sedimentary intervals (Hurst et al., 2003), influencing the distribution and efficiency of fluid migration, modifying reservoir shape and distribution, trap and seal properties, and forming excellent pay zones (Hurst and Cartwright, 2007; Braccini et al., 2008).

Studies of well-exposed outcrops of injection complexes (Vigorito et al., 2008; Scott et al., 2009, 2013) provide reliable geological context for such stratigraphic and petrological studies, and consistent analogues for subsurface interpretation (Hurst et al., 2015). For this reason, outcrop studies are fundamental to understand injectite features at sub-seismic and microscopic scales, serving as analogues for calibration of the subsurface petrofacies and of the plumbing systems they generate (Huuse et al., 2010).

Despite many studies on sediment remobilization and injection, and fluid flow processes of injectites (Cartwright et al., 2008; Huuse, 2008; Jackson et al., 2011), their smaller-scale features remain poorly documented and understood (cf., Duranti and Hurst, 2004; Huuse et al., 2007). Petrographic studies on sand injection complexes are still scarce and the understanding of the interrelationships between sediment remobilization and injection, and the post-injection diagenetic processes, is also at an early stage (e.g., Lonergan and Cartwright, 1999; Parnell and Kelly, 2003; Davies et al., 2006; Jonk et al., 2005; Jonk, 2010;Scott et al., 2009; Ravier et al., 2015;). Understanding the distribution of detrital composition and diagenetic alterations of sandstones and their impact on reservoir quality is crucial for petroleum exploration and production (Bloch and Helmold, 1995; De Ros and Goldberg, 2007; Morad et al., 2010). Petrofacies analysis of injectites is particularly valuable in subsurface interpretation where differentiation between depositional and injected sandstone may be challenging, even when excellent quality seismic and core data are available. Therefore, the characterization of petrofacies of sand injection complexes is fundamental in order to evaluate their reservoir characteristics ~~and their~~and their effects on fluid flow.

This study focuses on field investigations and petrographic analysis of the Tumey Giant Injection Complex (TGIC) in the Eocene succession of the San

Joaquin Basin (California, USA) (**Fig. 1**). The scarce previous works about the TGIC were focused on the outcrop features and external geometry (Huuse et al., 2007; Palladino et al., 2016, 2018) and recently on detailed lithostratigraphic mapping and structural analysis by Zvirtes et al. (2019). Here, we study the processes of sand remobilization and injection of the TGIC at meso- and micro-scales by detailed field and petrographic analysis, allowing the definition of the lithostratigraphic organization of the complex along with the description of primary composition, textures, diagenetic processes, provenance signatures, and petrofacies characteristics. The present study demonstrates the utility of the petrofacies concept to sand injection complexes and its aid for the definition of the petrogenetic relationships between intrusive sandstones and parent units, their characteristics in terms of reservoir petrofacies, and their impact on fluid flow.

2. Geological context

2.1. Tectonic setting

The TGIC crops out discontinuously along the western flank of the San Joaquin Basin, as part of the Great Valley Group (GVG), in Central California (Fig. 1). The GVG was deposited within a N-S elongate forearc basin system formed following the Nevadan orogeny in the Late Jurassic (Dickinson and Seely, 1979; Dickinson, 1981; Constenius et al., 2000). Throughout the Cretaceous and Paleogene, the eastward subduction of the oceanic Farallon plate beneath the continental North American plate (Atwater, 1970; Atwater and Stock, 1998), gave rise to the Franciscan-Great Valley-Sierra Nevada arc-trench system (Ingersoll, 1983) (Fig. 1A,B).

By the Late Cretaceous, the onset of the Laramide orogeny took place, due to the decreasing dip of the subducting slab, promoting eastward migration of the arc magmatism (Fig. 1B). This orogenic phase is considered to be responsible for the regional uplift of the GVG (Moxon and Graham, 1987). Subduction terminated by the late Paleogene and Neogene, by the northward movement of the Mendocino triple junction (Atwater, 1970) which shifted to the current transform margin of the western USA. The study area is part of the deformed western margin of the San Joaquin Basin, where the Cenozoic sequence was uplifted and exposed during Neogene contractional and strike-slip tectonics which developed the San Andreas Fault system (Atwater, 1970). This regime formed extensive arrays of NW-SE trending *en échelon* folds (Bartow, 1996) with alternating anticlines and synclines often underlain by thrust planes (Namson and Davis, 1988; Bartow, 1991), and NW-SE dextral faulting systems (Fig. 1C).

2.2. Petrologic evolution of the Great Valley forearc basin

The petrologic evolution of the GVG has been traced through many provenance studies (e.g., Dickinson and Rich, 1972; Mansfield, 1979, Dickinson et al., 1983; Ingersoll, 1983, 2012). Petrofacies of the GVG generally reflect the petrologic evolution of arc terranes, and unroofing of Sierran batholiths through the late Mesozoic (Ingersoll, 1983; Dickinson et al., 1983). Petrofacies document mainly the dissection of the Cretaceous Sierran magmatic arc, as well as the erosion of residual orogenic highlands formed during latest Jurassic arc–arc and arc-continent collision of the Nevadan orogeny (Ingersoll, 1983; Dickinson 2002). Vertical petrofacies changes of the GVG are recorded in the lithic sediments with sedimentary, volcanic and metamorphic grains from supracrustal sources in the lower portion of the sequence, related to erosion of the volcano-sedimentary cover of the Sierran magmatic arc, and older arc-derived terranes of the Nevadan orogeny. This succession evolved upward to arkosic sands derived from plutonic rocks as the volcanic cover of Sierra Nevada was stripped off, reflecting dissection of the magmatic arc to the east (Ingersoll, 1983).

During the Late Cretaceous-Early Paleogene, exhumation of the Sierra Nevada to the east, and uplift of the Franciscan Complex to the west took place (Unruh et al., 2007) (Fig. 1B), leading to changes in depositional environments, sedimentary palaeocurrent patterns and provenance, thus modifying the petrofacies characteristics of the succession. Palaeocurrent data from outcrops, facies distribution patterns, and provenance information suggest a predominantly westward, south-westward, and north-westward transport from the Sierran magmatic arc for most of the GVG (Ingersoll, 1979). This oblique and longitudinal sedimentary supply may have been controlled by bathymetric highs, the trench-slope break or outer arc ridges within the forearc basin. However, the occurrence of Franciscan-derived detritus within the Moreno Formation (Upper Cretaceous to Paleocene) (McGuire, 1988; Mitchell et al., 2010), and within part of the Domengine Formation (Middle Eocene) (Schulein, 1993; Sharman et al., 2017), suggests sedimentary contribution from the Franciscan Complex. These petrological variations throughout the sequence reflect the active tectonic environment of the basin and its subsequent influences over the sources and deposits of the GVG.

2.3. Stratigraphy of the study area

The study area is located in the northern portion of the Tumey Hills along the east margin of the Coast Ranges in Central California (Fig. 1C). This area records marine and non-marine deposition, with several unconformities associated with tectonic and eustatic fluctuations within the San Joaquin Basin (SJB) (Bartow, 1991, 1996; Johnson and Graham 2007). In the study area, ca. 650 m thick Paleocene to Miocene sedimentary sequences crops out, covering an area of approximately 4 km^2 (Fig. 2). The area is structured by an asymmetric anticline with a steeper limb dipping 30-50° to SW and a gentler limb dipping 20-30° to the NE (Zvirtes et al., 2019) (Fig. 2).

The oldest stratigraphic unit in the study sector is the Moreno Formation (Upper Cretaceous to Lower Paleocene), which consists of a sequence dominated by mudrocks and diatomaceous mudrocks, alternating with base-of-slope to shelf-edge turbiditic channels (Payne, 1951; McGuire, 1988) (Fig. 3). This formation hosts the Panoche Giant Injection Complex (Vigorito et al., 2008; Vigorito and Hurst, 2010), which is considered the biggest giant sand injection complex cropping out in the world. A regional unconformity that represents less than a 3 Ma hiatus (McGuire, 1988) eroding the top of the Moreno Formation. is overlain by the Lodo Formation. The Lodo Formation (Upper Paleocene to Lower Eocene) consists dominantly of claystone with sand-rich arkosic turbidites representing submarine slope to basin floor fans (Nilsen et al., 1974). During the Middle Eocene, the San Joaquin Basin became shallower, reflecting uplift and unroofing of the subduction complex (Moxon and Graham, 1987; Schulein, 1993; Johnson and Graham, 2007). Consequently, the coastline prograded, depositing estuarine and deltaic sediments of the Domengine Formation (Todd and Monroe, 1968; Sullivan and Sullivan, 2012; Sharman et al., 2017) (Fig. 3). At Tumey Hill, the Domengine Formation occurs as laterally discontinuous outcrops (10-30 m thick) of grey, highly bioturbated, very fine- to coarse-grained sandstones. Abrupt subsidence and basin-wide transgression led to a return of deep-marine conditions (Milam, 1985) resulting in widespread deposition of the Kreyenhagen Shale (Middle to Late Eocene). Milam (1985) suggests that the Domengine-Kreyenhagen boundary may represent a minor unconformity, with a depositional hiatus of less than 1 Ma.

The Kreyenhagen Shale is a widespread transgressive marine bathyal succession, which consists of fine-grained siliceous and calcareous biogenic facies, partially deposited under dysoxic to anoxic conditions (Milam, 1985). It is represented by siliciclastic and biosiliceous mudrocks, with intervals of porcelanite and diatomite. Locally, fine-grained deposits alternate with isolated, sand-rich slope channel-fills. Kreyenhagen Shale forms part of a major Paleogene slope deposited between 48 Ma and 36 Ma (Milam, 1985) and hosts the injectites of the Tumey Giant Injection Complex. The top of the formation, as well as the upper sector of the TGIC, is truncated by a Late Eocene unconformity, followed by the deposition of Late Eocene-Early Oligocene thick turbiditic Tumey Sandstone Lentil (Figs. 3 and 4), constraining the injection event to the Late Eocene (Zvirtes et al., 2019).

3. Materials and Methods

This study was based on detailed geological mapping of the TGIC, along with the petrographic analysis of the main lithological units associated with the sand injection complex. Stratigraphic intervals, geometries and spatial distribution of sandstone intrusions were mapped with support of photographs, satellite images, and stratigraphic profiles (Fig. 4A). Stratigraphic logs were used for petrofacies correlations and played an important role in differentiating between depositional and intrusive petrofacies, thereby allowing the definition of the lithostratigraphic organization of the complex (Fig. 4B).

Based on the relationships between sandstone intrusions and potential parent units of the Tumey Giant Injection Complex, 30 samples were selected for qualitative and quantitative petrographic and petrophysical analysis. We also analysed and compared the sandstones from the underlying Lodo and Domengine formations to investigate the geological influences on the Tumey Giant Injection Complex formation and their possible contribution of sand to the injection complex as potential parent units. Some samples were impregnated with blue epoxy resin prior to preparation of the thin sections to allow quantification of porosity. Selected samples were prepared for scanning electron microscopy analysis by secondary (SEM) and back-scattered electrons (BSE).

Quantification of primary and diagenetic constituents and porosity was obtained by quantitative petrographic analysis using the Gazzi-Dickinson method (Zuffa 1985) counting 300 evenly spaced points per section. The petrographic descriptions were acquired, stored and processed using the Petroledge® software (De Ros et al., 2007), which standardizes the geological nomenclature, allows reconstruction of the original composition, and provides automatic compositional classification and provenance detrital modes determination of sandstones. Detrital essential composition and provenance were displayed on Folk (1980) and Dickinson (1985) diagrams, respectively. Modification of clastic composition by hydrodynamic segregation and/or incorporation of host rock clasts into the intrusive sandstones framework, and textural modifications such as intragranular micro-fracturing, were also evaluated during petrographic analysis.

The sequence of diagenetic processes that affected the TGIC was defined based on textural paragenetic relationships among the diagenetic minerals observed through optical petrography and electron microscopy. Cross-cutting relationships between the different diagenetic constituents and their structures were used to reconstruct the relative chronology of each diagenetic phase. The composition, habits, textures, and fabric of siliciclastic and diagenetic constituents were also examined through scanning electron microscopy (SEM) with the support of energy-dispersive X-ray spectrometry (EDS) analysis, using a Carl Zeiss Gemini SEM 300 equipment at the University of Aberdeen. Particular emphasis was given to investigate grains surface textures, and intragranular micro-fractures mainly observed in sandstone intrusions.

4. Results and analysis

4.1. Internal organization of the TGIC

The TGIC is emplaced into the Kreyenhagen Shale (Middle to Upper Eocene), intruding a ca. 450 m thickness of mudrock and biosiliceous mudrock interbedded with sandstone-rich turbiditic channel-fills located at different stratigraphic positions (Figs. 4, 5). Based on stratigraphic and structural relationships, the TGIC is divided into lower and upper intrusive intervals (Zvirtes et al. 2019) (Fig. 5).

4.1.1. Lower intrusive interval

The lower intrusive interval occurs between ca. 480 m and 250 m below the Late Eocene unconformity. It is defined by: (1) an intrusive network dominantly composed of a sill complex with a stepped, staggered and multi-layered geometry connected by narrow, short low- and high-angle dykes; (2) host strata consist of ca. 250 m of brown, clay-rich mudrock intercalated with m-thick layers of biosiliceous mudrock; and (3) depositional sandstone, comprising channelized turbidites intensely modified by sand fluidization and feeding the adjacent intrusive network.

Depositional sandstone forms stacked turbiditic channel-fills, typically 1-4 m thick, but up to 8 m thick, extending laterally for 10's of meters (Figs. 5). They are grey, poorly to moderately sorted, medium-grained sandstone alternating with dm-thick intervals of brown mudrock (Fig. 6A). Medium-grained sand dominates, but pebbly conglomeratic sandstone occurs along channel bases with low-angle cross bedding shifting upward to sub-parallel bedding and structureless sandstone (Figs. 6A, C). Disruption of primary sedimentary structures is common, sometimes forming structureless units related to sand fluidization (cf., Zvirtes et al., 2019). Upper erosive margins are common, with the development of margin-parallel banding (Fig. 6B), which is a common feature in sand injectites (Scott et al., 2009; Hurst et al., 2011).

The architectural organization of the lower intrusive network is defined by a system of sills and low-angle intrusions, connected by planar and irregular dykes (Zvirtes et al., 2019). Sills commonly have discontinuous tabular geometry, with erosive lower and upper margins, and are individually up to 4 m-thick, but typically occur in the range of 0.5 to 2 m (Figs. 4, 5). Intrusions pinch-out laterally and have abrupt lateral changes in thickness, with planar and curved margins recording both brittle fracture of the host strata and erosion of host strata during sand emplacement. Mudrock clasts are common intra-clasts derived from the hydraulic fracture of the host strata. Dykes are discontinuous, volumetrically smaller, and more irregular than the sills. Short, high- to low-angle dykes <1 m thickness, typically show a thickness that range between 0.2 and 0.5 m, with planar and curved margins (Fig. 6C). Dykes bifurcate laterally and upwards where they form sub-vertical branches.

4.1.2. Upper intrusive interval

The upper intrusive interval (Zvirtes et al., 2019) occurs from ca. 250 m below the Late Eocene unconformity (Figs. 4 and 5). It consists of (1) host strata made up by clay-rich mudrock (ca. 50 m thick) that grade upward into bio siliceous-dominated mudrock (ca. 150 m thick); (2) depositional sandstone comprising sandy channel-fills, which are intensely modified by sand fluidization; and (3) an intrusive network of interconnected sills, dykes and injection breccia intruding ca. 200 m thickness of host strata and extending laterally for more than 2 km.

Depositional sandstone forms broader and thicker channel-fills (up to 40 m thick) than those in the lower intrusive interval (Figs. 4B, 7A). Typically, the channels have an amalgamated and homogeneous sandstone fill, without mud-rich interbeds. At the base of the channels, mudstone intra-clast lags occur formed by mass flows in the axial portion of the channels during deposition (Figs. 6E, F). The channels pass upward into thick homogeneous sandstone associated with intense sand fluidization (Zvirtes et al., 2019). Channels have direct contact with adjacent intrusions implying a common genetic relationship between both elements (Figs. 6D, 7).

Intrusions consist of composite dykes, sills, injection breccia and irregular intrusive bodies. They form a network of composite intrusions of asymmetric saucer-shaped intrusions with large wings emanating from the channelized turbidites (parent units) (Fig. 7). Dykes and sills intrude host strata at low and high angles and have a wide range of thickness (from 0.01 to 12 m). They occur in several intrusive shapes, ranging from sheet-like with planar margins to highly irregular, bulbous and curved margins (Zvirtes et al., 2019). Internal structures include banding (1 to 10 cm thickness) and laminae (0.2 to 1 cm thick), particularly developed in the margins and central portions of the intrusions. Bands are characterised by alignment of platy and elongate clasts, including fragments of mudrock derived from the host strata. A large-scale composite intrusion, up to 12 m thick, forms an impressive wing (*sensu* Huuse et al., 2007) displaying a series of steps with associated dykes and sills. The wing transects ca. 100 m of host strata and extends laterally more than 600 m from its parent unit (Figs. 5, 7). The geometry and scale of the wing is consistent with similar structures identified from interpretation of seismic data that frequently occur along the margins of turbiditic channels (Huuse et al., 2004; Jackson et al., 2011; Hurst and Vigorito, 2017; Zvirtes et al., 2019).

A broad injection breccia zone occurs exclusively in the upper intrusive interval (Zvirtes et al., 2019). It has an irregular and discontinuous sub-horizontal distribution, reaching a thickness of ca. 80 m, and extending laterally for hundreds of metres (Figs. 4, 8). Injection breccias consist of irregular sandstone intrusions among blocks of biosiliceous mudrock from ca. 0.01 to 3 m diameter, and irregular geometries (Fig. 8B) similar to the mudrock clast breccia (facies B4) of Duranti and Hurst (2004). The breccias form a range of complex lithofacies formed by breccias supported by clasts of biosiliceous mudrocks with a sandy matrix defined as “blocky breccias”, or breccias supported by a sandy matrix defined as “dispersive breccia” by Zvirtes et al. (2019). The sandy matrix presents a composition and grain size similar to the depositional and intrusive sandstones throughout the complex, suggesting a genetic relationship (Zvirtes et al., 2019).

Mudrock blocks are typically intruded by irregular dykes (0.1 to 3 m thick), and the resultant fractured clasts display a jig-saw texture (Duranti and Hurst 2004; Scott et al., 2009) (Fig. 8C, D). In the uppermost portion of the upper interval, there is a dyke-dominated zone, formed by low- and high-angle dykes with low aperture (0.1-0.5 m thick). This zone is eroded by the late Eocene unconformity, which in turn is overlain by turbiditic sandstones of the Tumey Sandstone Lentil (Zvirtes et al., 2019) constraining the injection event to the Upper Eocene (Figs. 4B, 5).

4.2. Petrographic analysis

To understand the petrogenetic relationships between depositional and intrusive sandstones, we defined petrofacies using field and petrographic data. The sandstone samples were classified in two broad petrofacies associations (**Fig. 9**): (1) depositional petrofacies from sandstones in the Lodo, Domengine, and Kreyenhagen formations; and (2) intrusive petrofacies, including dykes, sills and injection breccia. Sandstone primary detrital composition, diagenetic minerals and porosity (% of total rock volume) are presented in Table 1, with the recalculated modal point count data of detrital grains in Table 2.

4.2.1. Lodo Formation petrofacies

Structures, textures, and fabric. The Lodo Formation represents slope turbiditic sequence of fine-grained mudrock m- to dm-intercalated by turbiditic laterally-extensive fans (1-2 m thick). The samples consist of sub-mature, massive, fine- to medium-grained sandstones and discontinuous small lenses of bioclast-rich conglomerate (up to 50cm thick) (Fig. 10A). On average sandstones comprise 77% grains, 18% cement, and 5% porosity (Table 1). Grains are moderately to well sorted, with low sphericity. They are loosely packed with a homogeneous texture, which is preserved by early diagenetic, pre-compactional calcite cement (Figs. 10B, C). Framework grains are partially dissolved and have abundant point and rare long and concave-convex intergranular contacts. Intra-granular micro-fractures are rare (<2%) (Fig. 10D).

Primary composition. The detrital composition is arkosic (*sensu* Folk, 1980) (Fig. 11a) with mean QFL composition of Q46F40L14 (Table 2). Quartz grains are mainly monocrystalline quartz with sharp extinction, and to a lesser extent, monocrystalline quartz with wavy extinction. Polycrystalline grains are minor. Plagioclase is the dominant feldspar (Table 1), some with fractures and dissolution features, with less common orthoclase and microcline. Sedimentary rock fragments, mainly chert and mudrock, are the predominant lithic fragments, with subordinate volcanic and low rank metamorphic fragments, such as slate and phyllite.

Diagenetic constituents and porosity. Diagenetic processes and products identified in the Lodo Formation arkoses are pervasive pore-filling and grain-replacive poikilotopic calcite (Fig. 10C). Intrabasinal iron oxides and hydroxides occur as minor authigenic constituents. Local replacement of quartz and feldspar by calcite is observed (Fig. 10D). Intergranular macro-porosity (Table 1) is severely reduced by calcite cementation and the minor remaining porosity is mainly of secondary dissolution origin.

4.2.2. Domengine Formation petrofacies

Structures, textures, and fabric. Domengine Formation sandstones were deposited in deltaic and estuarine environments, and consist of 81% grains, 14% diagenetic cement, and 5% porosity (Table 1). Grain size ranges from very fine- to coarse-grained. Grains are well- to moderately-sorted, with mainly angular to sub-angular shape, and low sphericity (Fig. 10F, H). The grain fabric has normal packing, with chaotic to sub-parallel orientation. Intergranular contacts between grains are typically point and long, with rare concave-convex contacts. Similarly to the Lodo Formation samples, intra-granular micro-fractures are rare (<3% of grains).

Primary composition. Quartz-rich, lithic arkose is the detrital composition (sensu Folk, 1980; Fig. 11A). The mean QFL composition is Q65F21L14 (Table 2). Quartz is mainly monocrystalline with sharp extinction, with rare monocrystalline grains with wavy extinction, and polycrystalline grains (Table 1). K-feldspar is predominant over plagioclase. Lithic fragments are mainly derived from sedimentary rocks, composed mostly by chert and rare mudrock fragments. Volcanic rock fragments with aphyric and trachytic textures and metamorphic grains are subordinate (Table 1). Biotite, muscovite, and opaque and transparent heavy mineral grains are trace constituents.

Diagenetic constituents and porosity. The main observed diagenetic constituent corresponds to pervasive intergranular poikilotopic and coarse mosaic calcite (Fig. 10G, H). Structures associated with compaction include deformation of biotite and soft rock fragments. Rare discontinuous quartz, albite and K-feldspar overgrowths occur. Chlorite, iron oxides and hydroxides occur as replacements of undifferentiated detrital grains. Primary intergranular porosity was significantly reduced by calcite precipitation (Table 1), with minor secondary porosity created by cement dissolution.

4.2.3. Kreyenhagen Shale petrofacies

Structures, textures, and fabric. Sandstone in the Kreyenhagen Shale, representing marine slope channel-fills, consists of compositionally and texturally immature, moderately to mainly poorly sorted, very-fine to very-coarse, predominantly medium-grained sandstone (Figs. 9, 12). On average samples consist of 87% grains, 8% authigenic cement, and 5% porosity (Table 1). Grains are mainly angular to sub-angular, with low sphericity, and chaotic to sub-parallel orientation, marked by the long-axes of metamorphic and sedimentary rock fragments, biotite, muscovite, feldspars and quartz grains (Fig. 12C, F). Grain are normally packed with inter-granular point contacts predominating over long and concavo-convex contacts, with rare sutured contacts. Up to 10% of the grains have intra-granular micro-fractures (Table 1).

Primary composition. The primary composition of the Kreyenhagen sandstone is feldspathic litharenite (*sensu* Folk, 1980; Fig. 11A), rich in sedimentary and volcanic, and, to a lesser extent, low grade metamorphic rock fragments. The mean QFL composition is Q32F24L44 (Table 2). Quartz is mainly monocrystalline with abrupt extinction, and less commonly monocrystalline with wavy extinction. Subordinate polycrystalline quartz grains have granoblastic textures indicative of a metamorphic origin. K-feldspar dominates over plagioclase. Rock fragments, the main clastic component, comprise mostly chert and mudrock. Intermediate volcanic rock fragments with hemi-crystalline and trachytic textures marked by the alignment of laths of plagioclase (Fig. 12E) are also common. Metamorphic slate and schist grains are subordinate.

Diagenetic constituents and porosity. Intense mechanical compaction is pervasive with deformation of soft clasts, such as mudrocks, argillaceous intra-clasts, and mica grains (e.g., biotite), with concomitant lithic pseudo-matrix (Fig. 12C, F), and inter-granular cementation by poikilotopic gypsum (Table 1; Fig.12B). Authigenic clay coatings and chaotic pore-filling aggregates are common (Fig. 12D). The occurrence of discontinuous inter-granular pore-lining iron oxides and hydroxides is probably related to recent alteration associated with uplift and exposure (Fig. 12C). Porosity was greatly reduced by compaction and occluded by gypsum cementation, with minor secondary porosity formed by progressive dissolution of volcanic grains, mudrock clasts, clay mineral pseudomatrix and gypsum (Table 1).

4.2.4. Intrusive petrofacies: sandstone sills, dykes, and injection breccias

Structures, textures, and fabric.

On average, sandstone intrusions consist of 80% grains, 11% cement, and 9% porosity, with a fine-grained matrix present in some samples (Table 1). Samples are well- to dominantly moderately-sorted sandstones. Grains are very angular to sub-rounded, predominantly angular, with medium to low sphericity (Fig. 9). Sandstone is structureless or has irregular lamination marked by concentrations of rock fragments (Fig. 13), which are oriented parallel or sub-parallel to the intrusion margins. The fabric is loose to tightly packed, with grain orientation ranging from homogenous and chaotic to sub-parallel. Point intergranular grain contacts are more abundant than elongate contacts, with rare concavo-convex and sutured contacts.

Petrographic and BSE examination of the sandstone in the injection breccia zone reveals the pervasive presence of mudrock clasts with angular and rounded shapes and of varied sizes (Fig. 14A). Typically, sand grains penetrate the margins of mudrock clasts (Fig. 14), sometimes forming thin dykes (ca. 0.5 mm wide) (Fig. 14E).

The host biosiliceous mudrocks are rich in diatom frustules and radiolarian skeletons, still partially preserved as amorphous opal-A or recrystallized to opal-CT or micro-quartz with high degree of preservation (Fig. 14B). The process of corrasion (*sensu* Scott et al., 2009) is promoted by the erosion of host mudrock during sand injection (Figs. 14C-F). In some cases, clasts start to disintegrate to sand size and become part of the sand framework (Fig. 14C). These processes, along with scouring and erosion of the host strata, imply high-velocity turbulent flow conditions with low viscosity during sand injection (Scott et al., 2009; Hurst et al., 2011).

Primary composition. All the sandstone intrusions are feldspathic litharenites (*sensu* Folk, 1980) (Fig. 11A). The mean QFL composition is Q30F23L47 (Table 2). Quartz grains are intensely fractured, and mostly are composed of monocrystalline grains with abrupt extinction, subordinately by monocrystalline grains with wavy extinction, and polycrystalline grains with granoblastic texture of metamorphic origin (Table 1). Among the feldspars, which are commonly altered and fractured, K-feldspar dominates over plagioclase. Lithic fragments are the main detrital constituents of sandstone intrusions, with sedimentary fragments (mainly chert and mudrock) being the most abundant (Table 1). Volcanic fragments with trachytic texture are more common than metamorphic rock fragments such as phyllite and slate. On average, sedimentary rock fragments are 7% more abundant in the sandstone intrusions than in the parent turbiditic units (Table 1). We attribute this to the incorporation of host mudrock fragments during sand intrusion by hydrofracturing and erosion of host mudrocks. Accessory detrital constituents include biotite, muscovite, hornblende, zircon, and opaque heavy minerals.

Diagenetic constituents and porosity. Mechanical compaction is the main diagenetic process recorded affecting the deformation of primary constituents such as biotite, mudrock and volcanic fragments (Fig. 11C). Additionally, mechanical compaction is the responsible for the extensive formation of lithic pseudomatrix. Pervasive cementation developed by pore-filling poikilotopic gypsum (Fig. 11B Table 1). Porosity of sandstone intrusions varies throughout the complex (Table 1). Original porosity was intensely reduced by compaction and by pervasive gypsum cementation during early diagenesis. Dissolution of gypsum cement (Fig. 13E), pseudomatrix (Fig. 13F), and lithic fragments, such as volcanic fragments commonly created secondary porosity.

Microfracturing. Intense intra-granular micro-fracturing is common in quartz, feldspar and sedimentary lithic fragments of intrusive sandstones (Fig. 15). Stains of iron oxides and hydroxides highlight micro-fractures in quartz and feldspar (Fig. 15C). Quartz grains typically contain randomly-oriented planar and arcuate fractures (Fig. 15A, G, H) that tend to be less intense nearer to grain margins (Fig. 15A, E). Micro-fractures in quartz are typically randomly oriented. In some quartz grains, flaked surfaces with multiple conchoidal fractures may record multi-cyclic inter-granular collisions (Fig. 15G, H). Plagioclase grains commonly have orthogonal micro-fracture patterns developed along and perpendicular to cleavage and polysynthetic twins (Fig. 15c). K-feldspar grains have some random fracture orientation but fractures develop preferentially along the cleavages. Chert and mudrock clasts also contain micro-fractures, and like the monocrystalline quartz grains, are more fractured in their inner portions (Fig. 15F).

4.3. Effects of compaction and cementation on porosity

Compaction and cementation are the main mechanisms of primary porosity reduction in sandstones (e.g., Ehrenberg, 1995; Makowitz et al., 2006), and understanding the controls on these processes has significant implications for reservoir quality prediction. In this section, we discuss the conditions of mechanical compaction and cementation of depositional and intrusive sandstones, and their impact on porosity of the TGIC. The proportion of primary porosity loss due to compaction *versus* cementation can be represented in Ehrenberg's diagram (Ehrenberg, 1989) (Fig. 16), which represents the intergranular volume (IGV) *versus* the intergranular cement percentage, assuming a value of 40% of the initial (depositional) porosity. Intergranular porosity values represented in the diagram for the analysed samples are overestimated, because initial porosity was smaller than 40%, due to the moderate sorting (Ehrenberg, 1989).

The diagram indicates that the original porosity of both depositional and intrusive petrofacies was reduced mainly by mechanical compaction (Fig. 16). The deposited sandstones were more affected by mechanical compaction than the intrusive sandstones, due mostly to the pervasive generation of pseudomatrix, what resulted in lower intergranular porosity (average 4%; max. 7%). On the other hand, intrusive sandstones were relatively less affected by mechanical compaction and more affected by cementation than the depositional bodies, which resulted in higher porosity values of the former (average 8.7%; max. 22%). The intergranular porosity of the Kreyenhagen channel-fills and intrusive sands were also reduced by gypsum cementation. The higher porosity of the intrusive sandstones may be explained by two factors: (1) the deposited sandstones were already suffering mechanical compaction during early burial, when sand injection took place; and (2) grain packing reorganization that took place during sand fluidization and remobilization (Hurst and Cronin, 2001). Both factors could have influenced the porosity differences between depositional and intrusive sandstones.

5. Discussion

5.1. Provenance Analysis

In common with other sandstones, the ultimate control on the composition of sandstones is the composition of source terranes and related weathering, processes of sedimentary transport and temporary storage in depositional systems, and further modification during burial diagenesis (Ingersoll, 1983; Dickinson, 1985). Sand injection promotes additional factors and processes, other than those related to depositional environments, that modify sandstone composition, such as grain comminution from high-velocity inter-granular collisions and corrasion (Scott et al., 2009), during entrained flow and erosion of material from hydraulically-fractured host strata (Scott et al., 2009; Hurst et al., 2011; Ravier et al., 2015). Commonly, sandstone intrusions are compositionally similar to their parent units, which allows a genetic correlation between them (Hurst et al., 2017). However, the incorporation of host strata material during sand injection may modify the composition of the sand during its emplacement (Hurst et al., 2011).

Sandstone in the Lodo, Domengine and Kreyenhagen formations records significant provenance variation through time, with contributions from basement uplift to magmatic arc sources (*sensu* Dickinson, 1985) (Fig. 11B). Arkoses in the Lodo Formation. has a provenance signature characteristic of erosion and uplift of a continental basement block to the south of the San Joaquin Basin (Ingersoll *et al*., 2012). This signature concurs with palaeocurrents of a northward-prograding submarine fan system during the early Paleogene (Nilsen et al., 1974). Quartz-rich lithic arkoses of the Domengine Formation were deposited in shallow marine, deltaic and estuarine depositional systems after regional shoaling during the Middle Eocene and record a major period of regression related to the uplift of the basin (Schulein, 1993). They have a provenance signature from a dissected magmatic arc characteristic of mixed sources (*sensu* Dickinson, 1985) (Fig. 11B). Therefore, changing from the basement uplift of Lodo sandstones towards a dissected magmatic arc provenance of Domengine and Kreyenhagen formations, records a tectonic reorganization of the basin. Contribution from the exhumed Franciscan Complex is a potential source area for the Domengine sandstones (Schulein, 1993; Sharman et al., 2017). Unfortunately, no depositional structures were observed in the structureless sandstones of the formation. The relative high quartz content can be related to pervasive autocyclic controls in the depositional system, such as the erosion and reworking of sedimentary deposits, a longer-distance transport system, and consequent deterioration of less resistant components, such as feldspar and lithic fragments.

The overlain Kreyenhagen Shale records the deepening of the basin with slope mudstone and channelized sandstones. This records a regionally significant transgression during a period of extensive subsidence of the GVG in which there was a return to deep-water depositional conditions. The channel-fills comprise feldspathic litharenites with provenance signature characteristic of a dissected magmatic arc (*sensu* Dickinson, 1985) (Fig. 11B). This provenance is compatible with palaeocurrent data that indicate derivation from the Sierran magmatic arc to the east, which was intensely uplifted throughout the Cenozoic (Ingersoll *et al*., 2012). The Kreyenhagen channels have a high content of rock fragments that can be considered the result of erosion of supra-crustal sources, high sedimentation rates, and short transportation distances (Schrank et al., 2017). Possibly this indicates direct supply from fluvial systems into a deep-water environment (Hurst and Morton, 2001). Low-grade metamorphic fragments likely come from the metamorphic terrane of the Sierra Nevada orogenic system. The high content of volcanic rock fragments can be related to the erosion of Jurassic volcano-sedimentary sections formed during the Nevadan orogeny or by erosion of Cenozoic volcanic terranes related to the Idaho magmatism (Sharman et al., 2015).

Sandstone intrusions are compositionally very similar to the Kreyenhagen sandstone being composed by feldspathic litharenites rich in sedimentary, volcanism and metamorphic rock fragments and provenance signatures of a dissected magmatic arc (Fig. 10B). These strong compositional and provenance similarities confirm the field observations that Lodo and Domengine sandstones did not contribute sand to the formation of the TGIC, and that turbiditic channels in the Kreyenhagen Shale were the sole parent units for injected sand.

5.2. Diagenetic evolution of the TGIC

The connections between the types of diagenetic processes and their distributions are the key to interpret the evolution of the diagenetic alterations through time, and their controls on reservoir quality and heterogeneity (Morad et al., 2010, 2012; Schrank et al., 2017). The recorded diagenetic products and processes allowed the correlation of the petrogenetic relationships between the depositional units and the sandstones intrusions. Diagenetic processes strongly affected the porosity of each unit and consequently the quality of the TGIC as reservoir. The regional burial history of the San Joaquin Basin indicates that the Eocene succession experienced a burial not exceeding 2.5 km depth and records significant uplift from the Oligocene to Miocene, until total exhumation was achieved (*He et al*., 2014). This means that the analysed sandstones were mostly affected by processes within the field of eodiagenesis, which occurred under the influence of depositional fluids at depths less than about 2 km (T > 70°C), and of shallow mesodiagenesis, at depths at 2-3 km and temperatures between 70°C and 100°C (Morad et al., 2000). The evolution of the main diagenetic products and processes of the TGIC and the underlying Lodo and Domengine formations is summarized in the Figure 17.

5.2.1. Diagenesis of Lodo and Domengine sandstones

Arkoses and lithic arkoses in the Lodo and Domengine formations experienced similar diagenetic evolution. Both units were pervasively cemented by calcite along with accompanying dissolution and replacement of framework grains (e.g., quartz, feldspar) during early diagenesis (Fig. 17). Eogenetic calcite cement dominates the eodiagenesis of many shallow marine siliciclastic sediments (Morad et al., 2010), but can be important in deep-marine settings too. Seawater and carbonate shells are the main sources of ions for early marine carbonate cements (Morad, 1998). Sandstone in the Lodo Formation grades laterally into conglomerates containing carbonate bioclasts, the dissolution of which is the probable source of the eogenetic carbonate cement. The shallow marine Domengine sandstone are often enriched in carbonate bioclasts, which could have acted as nuclei for calcite precipitation, and as a source of cement during burial. Carbonate cementation is normally more extensive in transgressive systems tract sandstones, particularly below parasequence boundaries, transgressive surfaces, and maximum flooding surfaces (Morad et al., 2010). The Domengine sandstones represent deltaic and estuarine deposits overlain by the deep-water mudrocks of the Kreyenhagen Shale in a transgressive systems tract regime. Therefore, this corresponds to a situation with high potential for extensive carbonate precipitation.

Mechanical compaction in the arkoses and lithic arkoses of Lodo and Domengine formations had limited development due to fabric stabilization by the precipitation of early calcite cements. As cemented sandstones are unlikely to undergo liquefaction or fluidization due to their framework stiffness and low porosity and permeability, the early eogenetic cementation of Lodo and Domengine sandstones prevented fluidization of these units, also creating barriers for fluid migration (Fig. 17).

5.2.2. Diagenesis of Kreyenhagen sandstones (parent units) and intrusive network of the TGIC

Soon after deposition of the turbiditic Kreyenhagen succession, overpressure conditions inside the channels led pore-fluid pressure to overcome lithostatic pressure, triggering hydrofracture of the host strata and simultaneously leading to sand fluidization and injection. After sand injection, the progressive burial of the complex led to mechanical compaction of parent units and the intrusive network. Compaction was more intense in the parent unit sandstones because of the lack of early diagenetic cement and their lithic composition. Normally, the compaction of lithic sandstone promotes strong deformation of ductile fragments, such as mudrock, volcanic and low-grade metamorphic rock fragments, which generates a pseudomatrix and inhibits early cementation. Authigenic clay minerals (probably smectite) coatings occur in the parent units (Fig. 12D) and are inferred to pre-date sand injection. Smectite coatings or rims are commonly related to the alteration of volcanic fragments and mafic minerals (e.g., biotite) (De Ros et al., 1997; Morad et al., 2010), which are common in the lithic Kreyenhagen sandstones.

Pervasive carbonate is a common diagenetic cement in injectites (Jonk et al., 2005), however, the TGIC is pervasively cemented by gypsum. Poikilotopic gypsum occurs as early diagenetic pore-filling cement in the Kreyenhagen parent units and in sandstone intrusions. It is interpreted as a product of fluid percolation through the complex (Fig. 17). Unfortunately, the gypsum cementation of the deep-marine Kreyenhagen sandstones and intrusions of the TGIC have no clear origin for this process. Gypsum precipitation in sandstones is normally eodiagenetic and related to brine in evaporitic environments (Glennie et al., 1978; Strong and Milodowski, 1987; Henares et al., 2014). However, saturation can be reached by alteration of volcanogenic material which releases large amounts of Ca to the porewaters (Hoareau et al., 2011). The volcanic-rich litharenites of Kreyenhagen Shale channel-fills are potential sources of volcanogenic material for alteration. The gypsum cementation, along with mechanical compaction destroyed the primary porosity of depositional and intrusive sandstones, making them barriers for fluid migration.

Late dissolution of primary and diagenetic constituents, along with precipitation of iron oxides and hydroxides, is probably the result of exposure of the rocks to surface or near-surface conditions, during percolation of meteoric waters (Fig. 17). The dissolution of primary and diagenetic products created significant secondary porosity, with values up to 22% in the injection breccia (Table 1). The localized precipitation of iron oxides and hydroxides, and clay minerals were a product of hydration and oxidation of iron-rich mineral, such as pyrite and biotite during telodiagenesis (Rodrigues and Goldberg, 201). Overall, the diagenetic history of the TGIC records intense eodiagenetic evolution influenced by its depositional environments, followed by progressive burial and ultimately late uplift and exhumation, driven by contractional tectonics.

5.3. Microtextural analysis

The disintegration of clasts from host mudrocks along with the embedding of individual sand grains in the intrusion walls provides evidence of erosion associated with the process of corrasion, as demonstrated in the Yellowbank Creek Injection Complex in California by Scott et al. (2009) and in the Vocontian Basin in France by Ravier et al. (2015). Corrasion is defined by Allen (1984) as the erosion promoted when grains impact a surface at high velocity, resulting in the detachment of clasts from that surface. The petrographic analysis confirms that corrasion is the one of the main mechanisms of erosion of host mudrocks of the TGIC (Figs. 14, 15). The detachment of mudrock clasts and subsequent abrasion by sand grains is the main factor associated with the enrichment of mudrock clasts in the intrusive petrofacies in relation to their parent sandstones (Fig. 15J). Scott et al. (2009) speculate that corrasion is also responsible for the development of erosional scours observed along the margins of injectites, which are not described in detail but commonly observed in sandstone intrusions of the TGIC.

Petrographic analysis also revealed that the grains from the sandstone intrusions are often severely affected by micro-fracturing (Fig. 15). Microfractures can be developed by different geological processes such as weathering, transportation of grains from source rocks to depositional environment (Boggs, 2009), mechanical compaction or tectonism during diagenesis (Makowitz et al., 2006), and meteorite impacts (Ferrière et al., 2009). Brittle grain deformation during burial forms fractures that are commonly wedge-shaped, with aligned spalling, and small-scale cataclasis (Makowitz et al., 2006). Microfracturing associated with meteorite impacts show a well-organized orientation as planar deformation structures (Trepmann, 2008). None of these patterns are shown by the grains of TGIC sandstone intrusions. Fractures in sandstone intrusions seem to be developed following the structure of monomineralic grains (quartz and feldspar) and rock fragments, without systematic relationships with neighbouring grains, as formed by burial or tectonic fracturing. Intragranular fracturing preceded gypsum cementation, given that fractures do not crosscut the intergranular gypsum cement. The intrusive petrofacies present higher percentages of micro-fractured grains (5-35%) than the depositional petrofacies of KS (5-10%) (Fig. 15J). This evidence indicates that the TGIC grain fractures where not generated *in situ* by mechanical compaction of the parent units and intrusions, but rather during sand injection emplacement.

Sands from the lowermost TGIC parent units may have been transported upward for ca. 400 m and laterally for at least hundreds of meters (Fig. 4). During granular flow grains are in constant movement which can induce intergranular interactions such as frictional sliding and collisions among grains and between the grains and the host rocks. The intragranular fracturing patterns observed in the sandstone intrusions is very heterogeneous, and can be controlled by different parameters such as the stiffness, strength, and friction coefficient of different grains with different shapes and sizes (Li et al., 2018). The stress related to this process can cause mechanical flexure or torsions of crystalline structures of some minerals through preferential fragile crystallographic directions (e.g., cleavages or twinning).

During sand injection, emplacement is likely to involve complex mechanisms which include multiple grain impacts, different types of grains and grain sizes, different grain velocities (turbulent flow) and collisional angles. The pattern of intragranular fractures in intrusion sandstones associated with their angular fractured margins, and the abnormal frequency and degree of their development, suggests that injected sand suffered intense intergranular collisions during turbulent flow. Such micro-fracturing pattern can be considered a possible diagnostic feature to identify sand injectites.

5.4. Fluid flow and reservoir petrofacies heterogeneity

Sand injectites represent an emerging play in deep-water environments and may be characterised by typically good reservoir quality, playing a major role in fluid flow (Jonk, 2010). Once emplaced, they may form preferential conducts for fluid migration, as well as intrusive traps, constituting porous and permeable reservoirs of considerable volume and introducing high interconnectivity among otherwise isolated depositional sandbodies (Hurst and Cartwright, 2007). Sandstone heterogeneity strongly influences reservoir performance by controlling fluid flow (Wardlaw and Cassan, 1979; Weber, 1982). Consequently, reservoir heterogeneity prediction is of prime importance for the planning and execution of hydrocarbon production strategies. Sand injectites can create permeable pathways for hydrocarbon migration and act as good reservoirs but, on the other hand, they are also prone to cementation which reduce their porosity and reservoir potential (Jonk, 2010). According to the definition of the diagenetic alterations of the TGIC through time, we can estimate when the sand injections and related depositional succession behaved as potential fluid flow pathways and/or barriers (Fig. 17).

Sand fluidization and remobilization occurred only in the Kreyenhagen Shale turbidites, implying that supra-lithostatic conditions were attained just inside this unit and not in the underlying formations. Absence of fluidization of the Domengine and Lodo formation sandstones was probably a response to their early calcite cementation. Pervasive early cementation inhibits further mechanical compaction and can compartmentalize reservoirs by acting as barriers to water (and hydrocarbon) flow (Morad et al., 2010). Furthermore, the compaction of sandstone sequences containing zones with laterally continuous carbonate cementation may lead to the development of overpressure in adjacent, weakly cemented zones (Morad, 1998). In this context, the early calcite cementation of Domengine and Lodo formations could have acted as an underlying barrier, constraining fluid escape to the weakly cemented, porous Kreyenhagen channel-fills, thus promoting overpressure build up (Fig 17, time 1). On the other hand, the channel-fills of the Kreyenhagen Shale sealed by low permeability muddy strata were intensely fluidized and remobilized by overpressured fluids.

Before sand injection, the Kreyenhagen Shale channel-fills were under shallow burial, affected by progressive mechanical compaction, with sealing mudrocks preventing connate fluids to escape supporting overpressure build up. As the pore-fluid pressure overcame the fracture gradient of the host mudrocks, hydraulic fracture propagation was initiated and a pressure gradient between the overpressured sands and the lower-pressure upper interval was formed (Hurst et al., 2011). To balance this pressure gradient, overpressured fluid flow migrated to lower pressure zones. When the fluid flow overcame the minimum fluidization velocity of the sediments, sand fluidization and remobilization started, injecting fluidized sand into the fractured host mudrocks (Vigorito and Hurst, 2010) (Fig. 17, time 2). Hydraulic fracture propagation and sand injection eventually ceased when the pressure was balanced, stopping fluid flow. As the upper portion of the TGIC was eroded, we do not have evidence to determine whether the injections reached the paleo-seafloor or remained trapped in the shallow subsurface.

After emplacement, the intrusive network formed a network of pathways for fluid migration. Sand injections are reported to maintain relatively good porosity during shallow burial (Hurst and Cartwright, 2007), and the TGIC confirms this tendency because the intrusive network is overall more porous than its deposited parent units (Fig. 16). After sand injection, limited mechanical compaction followed by pervasive gypsum cementation caused heterogeneous but significant porosity reduction, creating barriers inside the complex (Fig. 17, time 3). Gypsum veins filling fractures and joints that cross the cemented sandstones may suggest multiple fluid overpressure episodes, or simply differential compaction and deformation during burial.

The last phase affecting the complex is associated with the Late Paleogene-Neogene exhumation of San Joaquin Basin. Significant oxidation (oxides and hydroxides) and dissolution of primary constituents, pseudomatrix, argillaceous intraclasts, and gypsum was promoted by the circulation of meteoric water within both the depositional and injected sandstones. This exhumation created pervasive secondary porosity, increasing fluid flow and consequently improving final reservoir quality (Fig. 17, time 4).

The diagenetic processes observed in the TGIC suggest that despite sand injections it usually has good porosity and may constitute good reservoirs. However, post-injection compaction, cementation and dissolution may change significantly the porosity and reservoir quality of injectites through time.

6. Conclusions

This study determined the stratigraphic organization and the petrogenetic relationships between depositional and intrusive petrofacies of the TGIC. It also evaluated how the diagenetic processes and reservoir petrofacies characteristics of sand injection complexes may vary through time. These results are important to understand injection complex architecture and petrofacies association, which can be used to model the flow of petroleum and aqueous fluids within injectite networks. The key conclusions resulting from this study are as follows:

(1) The pattern of compositional and textural parameters within the succession and its provenance signatures indicated that the sand supply to shallow and deep-water sandstones was constrained by the depositional geodynamic

evolution of the San Joaquin Basin during the early and middle Paleogene, associated with active tectonic setting and eustatic sea-level fluctuations.

(2) Field observations and petrofacies associations indicate that the parent units for the intrusive network were the turbiditic channels of the Kreyenhagen Formation without contribution from the underlying Lodo and Domengine formations.

(3) The injection of fluidised sand into hydrofractures resulted in the emplacement of a network of porous and permeable conduits of dykes, sills and breccias within thick impermeable strata, creating a porous plumbing system well-connected horizontally and vertically for fluid migration and diagenetic processes.

(4) Intrusive petrofacies are more porous than depositional parent units, presenting better reservoir quality.

(5) Corrasion is identified as an important process of erosion of host mudrocks.

(6) Intense intragranular micro-fracturing of quartz, feldspars and lithic fragments is assumed to have formed during fluidization and injection of sand, through intergranular collisions, and can be considered a potential diagnostic feature of sand injectites.

(7) Differential diagenetic processes influenced overpressure conditions and fluid migration, by creating flow barriers in the underlying units (early calcite

cementation of Lodo and Domengine formations), aiding lateral fluid migration into Kreyenhagen channel-fills. Post-injection compaction and gypsum cementation of intrusions and parent units reduced primary porosity, followed by telodiagenetic processes leading to intense cement dissolution by meteoric water, developing secondary porosity.

Acknowledgements

The authors gratefully acknowledge support from Shell Brazil and CNPq through the "BG05: UoA-UFRGS-SWB Sedimentary Systems" project at UFRGS and UoA and the strategic importance of the support given by ANP through the R&D levy regulation. We thank all the support from the Sand Injection Research Group (SIRG). We also wish to thank the support of the Bureau of Land Management (CA - USA) providing legal access to the study area.

References

Allen, J.R.L., 1984. Sedimentary Structures: Their Character and Physical Basis, 2 volumes. Developments in Sedimentology 30, Amsterdam, Elsevier, 663 pp.

Archer, J.B., 1984. Clastic intrusions in deep-sea fan deposits of the Rosroe formation, lower Ordovician, western Ireland. Journal of Sedimentary Petrology 54, 1197–1205.

Atwater, T., 1970. Implications of Plate Tectonics for the Cenozoic Tectonic Evolution of Western North America. GSA Bulletin 81, 3513–3536.

Atwater, T., Stock, J., 1998. Pacific-north America plate tectonics of the Neogene southwestern United States: An update: International Geology Review 40, 375–402.

Bartow, J.A., 1991. Cenozoic evolution of the San Joaquin Valley, California. U.S. Geological Survey, Professional Paper 1501, 40 pp.

Bartow, J.A., 1996. Geologic map of the west border of the San Joaquin Valley in the Panoche Creek–Cantua Creek area, Fresno and San Benito counties, California. Miscellaneous Investigations Series, US Geological Survey Map, I-2430.

Bergslien, D., 2002. Balder and Jotun - two sides of the same coin? A comparison of two Tertiary oil fields in the Norwegian North Sea. Petroleum Geoscience 8, 349–363.

Bloch, S., Helmold, K.P., 1995. Approaches to predicting reservoir quality in sandstones. American Association of Petroleum Geologists Bulletin 79, 97–115.

Boehm, A., Moore, J.C., 2002. Fluidized sandstone intrusions as an indicator of Paleostress orientation, Santa Cruz, California. Geofluids 2, 147–161.

Boggs., S.J. 2009. Petrology of Sedimentary Rocks. 2nd Edition. Cambridge University Press, Cambridge.

Braccini, E., de Boer, W., Hurst, A., Huuse, M., Vigorito, M., Templeton, G., 2008. Sand Injectites. Oilfield Review, 34–49 pp.

Cartwright, J., 2010. Regionally extensive emplacement of sandstone intrusions: A brief review. Basin Research 22, 502–516.

Cartwright, J., Huuse, M., Aplin, A., 2007. Seal bypass systems. AAPG Bulletin 91, 1141–1166.

Cartwright, J., James, D., Huuse, M., Vetel, W., Hurst, A., 2008. The geometry and emplacement of conical sandstone intrusions. Journal of Structural Geology 30, 854–867.

Constenius, K.N., Johnson, R.A., Dickinson, W.R., Williams, T.A., 2000. Tectonic evolution of the Jurassic-Cretaceous Great Valley forearc, California: Implications for the Franciscan thrust-wedge hypothesis Bulletin of the Geological Society of America 112, 1703–1723.

Davies, R.J., Huuse, M., Hirst, P., Cartwright, J., Yang, Y., 2006. Giant clastic intrusions primed by silica diagenesis. Geology 34, 917–920.

De Ros, L.F., Morad, S., Al-Aasm, I.S., 1997. Diagenesis of siliciclastic and volcaniclastic sediments in the Cretaceous and Miocene sequences of the NW African margin (DSDP Leg 47A, Site 397). Sedimentary Geology 112, 137–156.

De Ros, L.F., Goldberg, K., 2007. Reservoir petrofacies: a tool for quality characterization and prediction. American Association of Petroleum Geologists, Annual Convention and Exhibition, Long Beach, California 50055, 1–6.

De Ros, L.F., Goldberg, K., Abel, M., Victoreti, F., Mastella, M., Castro, E., 2007. Advanced acquisition and management of petrographic information from reservoir rocks using the Petroledge® System. AAPG Annual Convention and Exhibition, Long Beach, Expanded Abstracts.

Dickinson, W.R., 1981. Plate tectonics and the continental margin of California. In: Ernst, W.G. (Ed.), The geotectonic development of California. Englewood Cliffs, Prentice-Hall, pp. 1–28.

Dickinson, W.R., 1985. Interpreting provenance relations from detrital modes of sandstones. In: Zuffa, G.G. (Ed.), Provenance of Arenites. Dordrecht, Springer, pp. 333–361.

Dickinson, W.R., 2002. Reappraisal of hypothetical Franciscan thrust wedging at Coalinga: Implications for tectonic relations along the Great Valley flank of the California Coast Ranges. Tectonics, 21, p. 1039.

Dickinson, W.R., Rich, E., 1972. Petrologic intervals and petrofacies in the Great Valley Sequence, Sacramento Valley, California. GSA Bulletin 83, 3007-3024.

Dickinson, W.R., Beard, L.S., Brakenridge, G.R., Erjavec, J.L., Ferguson, R.C., Inman, K.F., Knepp, R.A., Lindberg, F.A., Ryberg, P.T., 1983. Provenance of North American Phanerozoic sandstones in relation to tectonic setting. Geological Society of America Bulletin, 94 (2), 222–235.

Dickinson, W.R., Seely, D.R., 1979. Structure and Stratigraphy of Forearc Regions. AAPG Bulletin 63, 2–31.

Diller, J.S., 1890. Sandstone dikes. Geological Society of America Bulletin 1, 411–442.

Dixon, R.J., Schofield, K., Anderton, R., Reynolds, A.D., Alexander, R.W.S., Williams, M.C., Davies, K.G., 1995. Sandstone diapirism and clastic intrusion in the Tertiary submarine fans of the Bruce-Beryl Embayment, Quadrant 9, UKCS. In: Hartley, A. J., Prosser, D. J., (Eds.) Characterization of Deep Marine Clastic Systems. Geological Society, London, Special Publications v. 94, 77–94.

Duranti, D., Hurst, A., 2004. Fluidization and injection in the deep-water sandstones of the Eocene Alba Formation (UK North Sea). Sedimentology 51, 503–529.

Ehrenberg, S.N., 1989. Assessing the relative importance of compaction processes and cementation to reduction of porosity in sandstones: Discussion; Compaction and porosity evolution of Pliocene sandstones, Ventura Basin, California: Discussion: American Association of Petroleum Geologists, Bulletin 73, 1274–1276.

Ferrière, L., Morrow, J.R., Amgaa, T., Koeberl, C., 2009. Systematic study of universal-stage measurements of planar deformation features in shocked quartz: Implications for statistical significance and representation of results. Meteoritics and Planetary Science 44, 925–940.

Folk, R.L., 1980. Petrology of Sedimentary Rocks. Hemphill Publishing Company, Austin, Texas, 182 pp.

Glennie, K.W., Mudd G.C., Nagtegaal, P.J.C., 1978. Depositional environment and diagenesis of Permian Rotliegendes sandstones in Leman Bank and Sole Pit areas of the UK southern North Sea. Journal of the Geological Society, London 135, 25-34

He, M., Graham, S., Scheirer, A.H., Peters, K.E., 2014. A basin modelling and organic geochemistry study in the Vallecitos syncline, San Joaquin Basin, California: Marine and Petroleum Geology 49, 15–34.

Henares, S., Caracciolo, L., Cultrone, G., Fernández, J., Viseras, C., 2014. The role of diagenesis and depositional facies on pore system evolution in a Triassic outcrop analogue (SE Spain). Marine and Petroleum Geology 51, 136-151

Hiscott, R.N., 1979. Clastic sills and dikes associated with deep-water sandstones, Tourelle formation, Ordovician, Quebec. Journal of Sedimentary Petrology 49, 1–10.

Hoareau, G., Monnin, C., Odonne, F., 2011. The stability of gypsum in marine sediments using the entire ODP/IODP porewater composition database. Marine Geology 279, 87–97.

Hurst, A., Morton, A.C., 2001. Generic relationships in the mineral-chemical stratigraphy of turbidite sandstones. Journal of the Geological Society 158, 401–404.

Hurst, A., Cronin, B.T., 2001. The origin of consolidation laminae and dish structures in some deep-water sandstones. Journal of Sedimentary Research 71, 136–143.

Hurst, A., Cartwright, J.A. (Eds.), 2007. Implications for Hydrocarbon Exploration and Production: American Association of Petroleum Geologists Memoir, Tulsa. 274 pp.

Hurst, A., Vigorito, M., 2017. Saucer-shaped sandstone intrusions: An underplayed reservoir target. AAPG Bulletin 101, 625–633.

Hurst, A., Cartwright, J.A., Duranti, D., 2003. Fluidization structures produced by upward injection of sand through a sealing lithology. In: Van Rensbergen, P., Hillis, R.R., Maltman, A.J., Morley, C.K. (Eds.), Subsurface Sediment Mobilization. Geological Society, London, Special Publication 216. pp. 123–138.

Hurst, A., Scott, A., Vigorito, M., 2011. Physical characteristics of sand injectites: Earth-Science Reviews 106, 215–246.

Hurst, A., Huuse, M., Duranti, D., Vigorito, M., Jameson, E., Schwab, A., 2015. Application of outcrop analogues in successful exploration of a sand injection complex, Volund Field, Norwegian North Sea. In: Bowman, M., Smyth, H.R., Good, T.R., Passey, S.R., Hirst, J.P.P., Jordan, C.J. (Eds.), The Value of Outcrop Studies in Reducing Subsurface Uncertainty and Risk in Hydrocarbon Exploration and Production. Geological Society, London, Special Publications 436, 75-92.

Hurst, A., Morton, A., Scott, A., Vigorito, M. 2017. Heavy-mineral assemblages in sandstone intrusions: Panoche Giant Injection Complex, California, U.S.A. Journal of Sedimentary Research 87, 388–405.

Huuse, M., 2008. Sandstone intrusions: Implications for exploration and production. World Oil 229, 87–91.

Huuse, M., Duranti, D., Steinsland, N., Guargena, C.G., Prat, P., Holm, K., Cartwright, J.A., Hurst, A., 2004. Seismic Characteristics of Large-Scale Sandstone Intrusions in the Paleogene of the South Viking Graben, UK and Norwegian North Sea. In:

Davies, R.J., Cartwright, J.A., Stewart, S.A., Lappin, M., Underhill, J.R. (Eds.), 3D Seismic Technology: Application to the Exploration of Sedimentary Basins. Geological Society, London, Memoirs 29, 263–278.

Huuse, M., J. Cartwright, A. Hurst, N. Steinsland, 2007. Seismic characterization of large-scale sandstone intrusions. In: Hurst A., Cartwright, J. (Eds.), Sand injectites: Implications for hydrocarbon exploration and production: AAPG Memoir 87, 21– 35.

Huuse, M., Jackson, C.A.L., Van Rensbergen, P., Davies, R.J., Flemings, P.B., Dixon, R.J., 2010. Subsurface sediment remobilization and fluid flow in sedimentary basins. An overview: Basin Research 22, 342–360.

Ingersoll, R.V., 1979. Petrofacies and petrologic evolution of the Late Cretaceous fore-arc basin, northern and central California. The Journal of Geology 86, 335–352.

Ingersoll, R.V., 1983. Petrofacies and Provenance of Late Mesozoic Forearc Basin, Northern and Central California: AAPG Bulletin 67, 1125–1142.

Ingersoll, R.V., 2012. Composition of modern sand and Cretaceous sandstone derived from the Sierra Nevada, California, USA, with implications for Cenozoic and Mesozoic uplift and dissection. Sedimentary Geology 280, 195–207.

Jackson, C.A.L., Huuse, M., Barber, G.P., 2011. Geometry of winglike clastic intrusions adjacent to a deep-water channel complex: Implications for hydrocarbon exploration and production. AAPG Bulletin 95, 559–584.

Johnson, C.L., Graham, S.A., 2007. Middle Tertiary stratigraphic sequences of the San Joaquin Basin, California: Chapter 6 in Petroleum systems and geologic assessment of oil and gas in the San Joaquin Basin Province, California. Professional Paper 1713-6.

Jolly, R.J.H., Lonergan, L., 2002. Mechanisms and controls on the formation of sand intrusions: Journal of the Geological Society 159, 605–617.

Jonk, R., 2010. Sand-rich injectites in the context of short-lived and long-lived fluid flow: Basin Research 22, 603–621.

Jonk, R., Hurst, A., Duranti, D., Parnell, J., Mazzini, A., Fallick, A.E., 2005. Origin and timing of sand injection, petroleum migration, and diagenesis in Tertiary reservoirs, south Viking Graben, North Sea. AAPG Bulletin 89, 329–357.

Li, X.F., Zhang, Q.B., Li, H.B., Zhao, J., 2018. Grain-Based Discrete Element Method (GB-DEM) Modelling of Multi-Scale Fracturing in Rocks Under Dynamic Loading. Rock Mechanics and Rock Engineering 51, 3785–3817.

Lonergan, L., Cartwright, J.A., 1999. Polygonal faults and their influence on deep-water sandstone reservoir geometries, Alba field, United Kingdom central North Sea: AAPG Bulletin (American Association of Petroleum Geologists) 83, 410–432.

Ma, G., Zhang, Y., Zhou, W., Ng, T.T., Wang, Q., Chen, X., 2018. The effect of different fracture mechanisms on impact fragmentation of brittle heterogeneous solid: International Journal of Impact Engineering 113, 132–143.

Makowitz, A., Lander, R.H., Milliken, K.L., 2006. Diagenetic modelling to assess the relative timing of quartz cementation and brittle grain processes during compaction. AAPG Bulletin 90, 873–885.

McGuire, D.J., 1988. Stratigraphy, depositional history, and hydrocarbon source-rock potential of the Upper Cretaceous–Lower Tertiary Moreno Formation, Central San Joaquin basin, California. (Ph.D. thesis) Stanford University, CA. 309 pp.

MacLeod, M.K., Hanson, R.A., Bell, C.R., McHugo, S., 1999. The Alba Field ocean bottom cable seismic survey: Impact on development. The Leading Edge 18, 1306–1312.

Makowitz, A., Lander, R.H., Milliken, K.L., 2006. Diagenetic modelling to assess the relative timing of quartz cementation and brittle grain processes during compaction. AAPG Bulletin 90, 873–885.

Mansfield, C.F., 1979. Upper Mesozoic subsea fan deposits in the southern Diablo Range, California: record of the Sierra Nevada magmatic arc. GSA Bulletin 90, 1025-1046.

Milam, R., 1985. Biostratigraphy and sedimentation of the Eocene and Oligocene Kreyenhagen Formation, central California. (Ph.D. thesis), Stanford University, 240 p.

Mitchell, C., Graham, S.A., Suek, D.H., 2010. Subduction complex uplift and exhumation and its influence on Maastrichtian forearc stratigraphy in the Great Valley Basin, northern San Joaquin Valley, California. Bulletin of the Geological Society of America 122, 2063–2078.

Morad, S., 1998. Carbonate cementation in sandstones: distribution patterns and geochemical evolution. In Morad, S. (Ed.), Carbonate Cementation in Sandstones. International Association of Sedimentologists Special Publication 26, 1–26.

Morad, S., Ketzer, J.M., De Ros, F., 2000. Spatial and temporal distribution of diagenetic alterations in siliciclastic rocks: implication for mass transfer in sedimentary basins. Sedimentology 47, 95–120.

Morad, S., Al-Ramadan, K., Ketzer, J.M., and De Ros, L.F., 2010. The impact of diagenesis on the heterogeneity of sandstone reservoirs: A review of the role of depositional fades and sequence stratigraphy. AAPG Bulletin 94, 1267–1309.

Morad, S., Ketzer, J.M., De Ros, L.F., 2012. Linking Diagenesis to Sequence Stratigraphy: An Integrated Tool for Understanding and Predicting Reservoir Quality Distribution. In: Morad, S., Ketzer, J.M., De Ros, L.F. (Eds.), Linking Diagenesis to Sequence Stratigraphy. IAS Special Publication 45, 1–36.

Moxon, I.W., Graham, S.A., 1987. History and controls of subsidence in the Late Cretaceous-Tertiary Great Valley forearc basin, California. Geology 15, 626-629.

Murchison, R.I., 1827. On the coal field of Bora in Sutherlandshire and some other stratified deposits in the North of Scotland. Transactions of the Geological Society of London S-2, 293–326. https://doi.org/10.1144/transgslb.2.2.293.

Namson, J.S., Davis, T.L., 1988. Seismically active fold and thrust belt in the San Joaquin Valley, central California. Geological Society of America Bulletin 100, 257–273.

Newsom, J.F., 1903. Clastic dikes. Geological Society of America Bulletin 14, 227–268.

Nilsen, T.H., Dibblee, T.W., Jr., Simoni, T.R., Jr., 1974. Stratigraphy and Sedimentation of the Cantua Sandstone Member of the Lodo Formation, Vallecitos Area, California. In: Payne, M.B. (ed.), The Paleogene of the Panoche Creek-Cantua Creek Area, Central California: Pacific Section, Society of Economic Paleontologists and Mineralogists, Field Trip Guidebook, 38-68.

Palladino, G., Grippa, A., Bureau, D., Alsop, I.G., Hurst, A., 2016. Emplacement of sandstone intrusions during contractional tectonics. Journal of Structural Geology 89, 230–249.

Palladino, G., Alsop, G.I., Grippa, A., Zvirtes, G., Phillip, R.P., Hurst, A., 2018. Sandstone-filled normal faults: A case study from central California. Journal of Structural Geology 110, 86–101.

Parnell, J., Kelly, J., 2003. Remobilisation of sand from consolidated sandstones: evidence from mixed bitumen-sand intrusions. In: Van Rensburgen, P., Hillis, R.R., Maltman, A.J., Morley, C.K. (Eds.), Subsurface Sediment Mobilization. Geological Society, London, Special Publications 216, 505-513 pp.

Payne, M.B., 1951. Type Moreno Formation and overlying Eocene strata on the west side of the San Joaquin Valley, Fresno and Merced Counties. California Division of Mines, Geological Special Report 9, 42.

Pierre, C., 2017. Origin of the authigenic gypsum and pyrite from active methane seeps of the southwest African Margin. Chemical Geology 449, 158–164.

Ravier, E., Guiraud, M., Guillien, A., Vennin, E., Buoncristiani, J.F., Portier, E., 2015. Micro- to macro-scale internal structures, diagenesis and petrophysical evolution of injectite networks in the Vocontian Basin (France): Implications for fluid flow. Marine and Petroleum Geology 64, 125–151.

Rodrigues, A.G., Goldberg, K., 2014. Primary composition and diagenetic patterns of sandstones from Barra de Itiúba Formation in Atalaia High, Sergipe Sub-Basin. Brazilian Journal of Geology 44, 545–560.

Schrank, A.B.S., Altenhofen, S.D., De Ros, L.F., 2017. Diagenetic Preservation and Modification of Porosity in Aptian Lithic Reservoirs from the Sergipe–Alagoas Basin, NE Brazil. Journal of Sedimentary Research 87, 1156–1175.

Schwab, A.M., Jameson, E.W., Townsley, A., 2015. Volund Field: Development of an Eocene Sandstone Injection Complex, Offshore Norway. In: McKie, T., Rose, P.T.S., Hartley, A.J., Jones, D., Armstrong, T.L. (Eds.), Tertiary Deep-Marine Reservoirs of the North Sea Region. Geological Society of London, Special Publication 403, 1–16.

Schwartz, H., Sample, J., Weberling, K.D., Minisin, D., Moore, J.C., 2003. An ancient linked fluid migration system: cold-seep deposits and sandstone intrusions in the Panoche Hills, California, USA. Geo-Marine Letters 23, 340–350.

Schulein, B.J., 1993. Sedimentation and tectonics of the upper lower to lower middle Eocene Domengine Formation Vallecitos syncline, California. (M.Sc. thesis), Stanford, California, Stanford University, 343 pp.

Scott, A., Vigorito, M., Hurst, A., 2009. The Process of Sand Injection: Internal Structures and Relationships with Host Strata (Yellowbank Creek Injectite Complex, California, U.S.A.). Journal of Sedimentary Research 79, 568–583.

Scott, A., Hurst, A., Vigorito, M., 2013. Outcrop-based reservoir characterization of a kilometer-scale sand-injectite complex. AAPG Bulletin 97, 309–343.

Sharman, G.R., Graham, S.A., Grove, M., Kimbrough, D.L., Wright, J.E., 2015. Detrital zircon provenance of the late Cretaceous-Eocene California forearc: Influence of Laramide low-angle subduction on sediment dispersal and paleogeography. Bulletin of the Geological Society of America 127, 38–60.

Sharman, G.R., Schwartz, T.M., Shumaker, L.E., Trigg, C.R., Nieminski, N.M., Sickmann, Z.T., Malkowski, M.A., Hourigan, J.K., Schulein, B.J., Graham, S.A., 2017. Submarine mass failure within the deltaic Domengine Formation (Eocene), California (USA). Geosphere 13, 950–973.

Strong, G.E., Milodowski, A.E., 1987. Aspects of the diagenesis of the Sherwood Sandstones of the Wessex Basin and their influence on reservoir characteristics. In: Marshall, J.D. (Ed.), Diagenesis of Sedimentary Sequences. Geological Society Special Publication 36, 325-337.

Sullivan, R., Sullivan, M.D., 2012. Sequence Stratigraphy and Incised Valley Architecture of the Domengine Formation, Black Diamond Mines Regional Preserve and the Southern Sacramento Basin, California, U.S.A. Journal of Sedimentary Research 82, 781–800.

Surlyk, F., Gjelberg, J., Noe-Nygaard, N., 2007. The Upper Jurassic Hareelv Formation of East Greenland: A giant sedimentary injection complex. In: Hurst, A., Cartwright, J.A. (Eds.), Sand Injectites: Implications for Hydrocarbon Exploration and Production: American Association of Petroleum Geologists Memoir, Tulsa, pp. 141–149.

Surlyk, F., Noe-Nygaard, N., 2001. Sand remobilisation and intrusion in the Upper Jurassic Hareelv Formation of East Greenland. Bulletin of the Geological Society of Denmark 48, 169–188.

Todd, T.W., Monroe, W.A., 1968. Petrology of Domengine Formation (Eocene), at Potrero Hills and Rio Vista, California. Journal of Sedimentary Research 38, 1024–1039.

Trepmann, C.A., 2008. Shock effects in quartz: Compression versus shear deformation - An example from the Rochechouart impact structure, France. Earth and Planetary Science Letters 267, 322–332.

Unruh, J.R., Dumitru, T.A., Sawyer, T.L., 2007. Coupling of early Tertiary extension in the Great Valley forearc basin with blueschist exhumation in the underlying Franciscan accretionary wedge at Mount Diablo, California. Bulletin of the Geological Society of America 119, 1347–1367.

Vigorito, M., Hurst, A., 2010. Regional sand injectite architecture as a record of pore-pressure evolution and sand redistribution in the shallow crust: insights from the Panoche Giant Injection Complex, California. Journal of the Geological Society 167, 889–904.

Vigorito, M., Hurst, A., Cartwright, J.A., Scott, A., 2008. Regional-scale subsurface sand remobilization: geometry and architecture. Journal of the Geological Society 165, 609–612.

Wardlaw, N.C., Cassan, J. P., 1979. Oil recovery efficiency and the rock-pore properties of some sandstone reservoirs. Bulletin of Canadian Petroleum Geology 27, 117–138.

Weber, K.J., 1986. How heterogeneity affects oil recovery. In Lake, L. W., Carroll Jr., H. B. (Eds.), Reservoir characterization. New York, Academic Press, pp. 487– 544.

Zuffa, G.G., 1985. Optical analyses of arenites: influence of methodology on compositional results. In Zuffa, G.G., (Ed.), Provenance of Arenites. Dordrecht, Springer, pp. 165–189.

Zvirtes, G., Hurst, A., Philipp, R.P., Palladino, G., Grippa, A., 2019. The Tumey Giant Injection Complex, Tumey Hill, California (USA). In: Silcock, S., Huuse, M., Bowman, M., Hurst. A. & Cobain. S. (Eds.), Subsurface Sand Remobilization and Injection. Geological Society, London, Special Publications 493, 34 pp. https://doi.org/10.1144/SP493-2019-3

Figure Captions

Figure 1. Geological context overview and location of the study area (modified from Zvirtes et al., 2019). (A) Simplified geographic and geological map of North and Central

California. (B) W-E geological cross-sections showing the tectonic evolution of the Great Valley forearc basin from Late Cretaceous subduction system to the present transform regime of the San Andreas Fault system (modified from Dickinson and Seeley, 1979), and the relative position of the Tumey Giant Injection Complex (TGIC). (C) Regional geological map of the study area, with the relevant stratigraphic units (modified from Bartow, 1996); (D) Schematic NW-SE section along Tumey and Panoche Hills, showing the erosional truncation of progressively older stratigraphic units toward the west-northwest, and the relative position of Tumey Hill succession (modified from Sharman et al., 2017).

Figure 2. (A) Detailed geological map of the Tumey Hill area, with the main depositional and intrusive units (blue) of the Tumey Giant Injection Complex and location of the samples analysed in this paper. (B) W-E cross section of the Tumey Hill area (see map for location). Note that the sandstone intrusions (in blue) are schematically represented with exaggerated size, for visualization proposes.

Figure 3. (A) Generalized stratigraphic column for the Panoche and Tumey Hills area with the architectural organization of the Panoche Giant Injection Complex emplaced during the Early Paleocene into muddy strata of Moreno Formation (Vigorito et al., 2008), and of the Tumey Giant Injection Complex emplaced in the Kreyenhagen Shale. Abbreviations: Cret. = Cretaceous; Fm. = Formation; M = Middle; Sh. = Shale; Ss. = Sandstone. (modified from Johnson and Graham, 2007; Sharman et al., 2017). (B) Stratigraphic column of Tumey Giant Injection Complex at Tumey Hill area, with lithostratigraphic organization (above) and geometries of the main intrusive bodies of the complex (below).

Figure 4. (A) Satellite image (Google Earth) of Tumey Hill, with the location of the main log profiles presented in B (eye view is 40° to topographic surface toward East at 2.35

km altitude). (B) Stratigraphic log sections of Tumey Hill area, with geological interpretation and facies associations of the complex. Note that the intrusions between logs (blue) are schematically correlated for spatial and geometric visualization (modified from Zvirtes et al., 2019).

Figure 5. Schematic 3D block diagram representing the lithostratigraphic and architectural organization of the Tumey Giant Injection Complex, with relative location of the outcrops presented throughout the paper (modified from Zvirtes et al., 2019).

Figure 6. Outcrops of depositional turbiditic channel-fills (parent units) of Kreyenhagen Formation. (A) Modified depositional turbiditic sandstones (>6 m thick) with depositional and remobilization structures, overlain by brown clay-rich mudrocks being intruded by dykes and sills that emanate from the turbiditic body; (B) Detail of the upper erosional surface of the channel with development of sub-parallel banding; (C) Detail of the irregular and segmented sandstone dyke emanating from the underlying turbiditic sandstone; (D) Picture of the upper channel-fill feeding a wing-like intrusion; (E) Basal section the upper sandy channel-fill with preserved large-scale cross-bedding and conglomeratic basal lag marking erosional surface inside the channel; (F) Photo interpretation of € (modified from Zvirtes et al. (2019).

Figure 7. Upper intrusive interval of the Tumey Giant Injection Complex. (A) 3D block diagram of figure 5 with location of the wing-like intrusion system; (B) Panorama view of the upper intrusion interval showing the geographical location of the main parent unit (left), the related wing-like intrusion (right) and breccia zones (background); (C) Picture of the main outcrop zone of the wing-like intrusion and the host biosiliceous mudrocks; (D) Close view of the main steps of the wing-like intrusion with feeder dykes (below) connected with the thick intrusion steps (above) and breccias to the right.

Figure 8. Outcrops of the injection breccia zones. (A) Panoramic view of the injection breccia outcrop belt developed within biosiliceous mudrocks in the upper intrusive interval (white rocks) and respective stratigraphic log (right); (B) Biosiliceous mudrocks intensely brecciated and injected by medium-grained sandstone with mudrock clasts with varied shapes and sizes. Detail of gypsum veins filling fractures in the right; (C) Photo of matrix-supported injection breccia (dispersive breccia); (D) Photointerpretation of (C). Yellow: sandstone; Brown: Mudrock clasts; Blue: Gypsum veins.

Figure 9. Summary of the characteristics of depositional and intrusive petrofacies.

Figure 10 – Meso- and micro-scale characteristics of Lodo (A, B, C and D) and Domengine (E, F, G and H) sandstones. (A) Outcrop of Lodo Formation displaying intercalation of turbiditic sandstones, bioclasts-rich conglomerates , and dark brownish mudrocks. Log section to the left; (B) Photomicrographs of a well sorted, medium-grained arkose (uncrossed polarizers //P at top left; crossed polarizers XP at bottom right); (C) Arkose with pore-filling poikilotopic calcite cement (Cal) , obliterating primary porosity and replacing quartz (Qz), feldspars (Kf and Pl) and chert (Ch) grains (yellow arrows) (XP); (D) High magnification view of calcite cementation and replacement of plagioclase (Pl), K-feldspar (Kf) and quartz (Qz).(XP); (E) Outcrop of Domengine sandstone intensely modified by bioturbation with randomly orientated burrows (detailed in the top right); (F) Photomicrographs of shallow marine, well sorted, very fine-grained lithic arkose, with glauconite pellets (uncrossed polarizers //P at top left ; crossed polarizers XP at bottom right); (G) Lithic arkose of Domengine Formation rich in quartz, K-feldspar and chert fragments cemented by calcite (XP) (H) Detail of pervasive pore-filing calcite cementation (XP).

Figure 11. Petrological characteristic of the depositional and intrusive sandstones and their petrogenetic associations. (A) Detrital composition of sandstones plotted in Folk

(1968) diagram; (B) Provenance diagram (Dickinson, 1985), showing the variation of sources between depositional sandstones and correlation with intrusive petrofacies. Note the petrogenetic association between Kreyenhagen channel-fills (orange circles) and sandstone intrusions (yellow circles), suggesting a common genetic origin.

Figure 12. Photomicrographs of the Kreyenhagen sandstones (parent units). (A) Photomicrographs (parallel: //P and crossed polarizers: XP) of sample 06: poorly sorted, fine- to medium-grained feldspathic litharenite, rich in sedimentary, volcanic and low-grade metamorphic rock fragments (yellow arrow); (B) Pervasive pore-filing gypsum (Gy) cementation in sandstone with quartz (Qz), K-feldspar (Kf), plagioclase (Pl) grains, volcanic (Volc) and metamorphic rock fragments of phyllite (Phy); (XP); (C) Intense mechanical compaction of biotite and mudrock fragments, with formation of pseudomatrix (yellow arrows)(//P); (D) Pore-lining and grain coatings authigenic clays (probably smectite) inhibiting gypsum cementation; (XP); (E) Volcanic rock fragment with trachytic texture; (XP); (F) Argillaceous pseudomatrix developed by intense mechanical compaction and deformation of mud intraclasts and micas; (//P).

Figure 13. Photomicrographs of the sandstone intrusions. (A) Photomicrographs (//P and XP) of moderately sorted feldspathic litharenite rich in sedimentary (chert and mudrock), volcanic and low-grade metamorphic rock fragments. (B) Pervasive pore-filing poikilotopic gypsum (Gy) cementation. Chert (Ch) and phyllite (Phy) fragments. (XP). (C) Intense mechanical compaction and pseudomatrix development from deformation of biotite and mudrock fragments (XP). (D) Quartz, feldspars and chert grains cemented by poikilotopic gypsum cement. Note the strong intragranular micro-fracturing of some quartz and feldspars (XP). (E) Lithic sandstone with alignment of biotite and mudrock fragments. Secondary porosity created by dissolution of gypsum cement. Note the intense grains fracturing, especially the quartz grains in the bottom left of the picture

(//P). (F) Dissolution of argillaceous pseudomatrix, gypsum cement, and biosiliceous fragments (centre) generating secondary porosity (//P).

Figure 14. Photomicrographs of sandstone intrusion in the breccia zone. (A) Mudrock clast injection breccia (sample 85) with angular and rounded fragments of biosiliceous mudstones with wide range of sizes, surrounded by a matrix of medium-grained sand; (//P); (B) Host biosiliceous mudrock (//P) rich in diatoms (bottom left; //P) and radiolarians (top right; XP) preserved as amorphous opal-A and micro-crystalline opal-CT; (C) Biosiliceous mudrock fragment being disintegrated by sand injection (corrasion), generating an input of sand size host strata fragments to the injected sandstones (//P); (D) Detail of penetration of sand grains in the margins of mudrock fragment. Note development of secondary porosity associated with dissolution of gypsum cement, feldspar grains and volcanic rock fragments (yellow arrows; //P); (E) Micro-dike of sand injection into host biosiliceous mudrock. Note deformation of the host biosiliceous material close to embedded grains (yellow arrows; //P); (F) SEM image of and embedded quartz grain into host biosiliceous mudstone. Note intragranular microfracture crossing the grain (yellow arrow).

Figure 15. (A) Photomicrograph of a sandstone dyke (sample 40A), with grains of quartz (yellow arrows) and feldspar (red arrow) with intense intragranular micro-fracturing (XP); (B) Photomicrograph of a micro-fractured large grain of chert (centre)(//P); (C) Photomicrograph of a sandstone sill (sample 38A) with up to 35% of the grains micro-fractured. Note orthogonal fracture pattern along crystalline structure of plagioclase (Pl); (D) Two quartz grains highly fractured with very irregular and sharp margins (BSE); (E) Strongly micro-fractured quartz grains (BSE); (F) Micro-fractured feldspar (BSE); (G) Quartz grain with multiple conchoidal fracture surfaces associated with intense intergranular collisions (SEM); (H) Quartz grain with flaked surface marked by conchoidal fractures (SEM); (I) BSE image of micro-fractured quartz grain embedded in biosiliceous

mudrock; (J) Schematic conceptual model for the processes of corrasion of host rocks and micro-fracturing of clastic grains during sand remobilization from parent units and intrusion into opening fracture system.

Figure 16. Ehrenberg diagram (Ehrenberg, 1989) showing the relationship between total intergranular volume and intergranular cement of sandstones, as evaluation of the porosity reduction by cementation and/or compaction of depositional and intrusive petrofacies. Note that the sandstone intrusions present a more porous petrofacies characteristic than their parent units of Kreyenhagen channel-fills that were more affected by mechanical compaction presenting a strongly compacted petrofacies characteristic.

Figure 17 – Diagenetic and petrological evolution of the Tumey Giant Injection Complex and its impact on fluid flow. Board displaying the diagenetic sequence of depositional and intrusive petrofácies (top left). Lodo and Domengine petrofacies present similar diagenetic evolution therefore are shown at the same evolutionary diagenetic sequence (lower portion of the board). The same is applied to the sandstone intrusions and parent unit of Kreyenhagen Shale. The sequence of the main diagenetic processes affecting the Tumey Giant Injection Complex are represented in the schematic geological sections 1 to 4.

Table Captions

Table 1. Detrital, diagenetic and porosity amounts (% of total rock volume) of deposited and intrusive sandstones, along with % of microfractured grains. (Grain parameters: Qm = monocrystalline quartz; Qp = polycrystalline quartz; K = K-feldspar; P = plagioclase; F = K + P; Lv = volcanic fragments; Ls = sedimentary fragments; Lm = metamorphic fragments; M = micas).

Table 2. Recalculated modal point count data for the intrusive sandstones of the Tumey Giant Injection Complex and deposited sandstones of the Kreyenhagen formation, and sandstones of the Lodo and Domengine formations. (Av., average; SD. standard deviation. Grain parameters: Qm = monocrystalline quartz; Qp = polycrystalline quartz; Qt = Qm + Qp; K = K-feldspar; M = phyllosilicates; P = plagioclase; F = K + P; L = aphanitic lithic grains; Lt = L + Qp; Lv = volcanic fragments; Ls = sedimentary fragments; Lm = metamorphic fragments).

Fig. 1

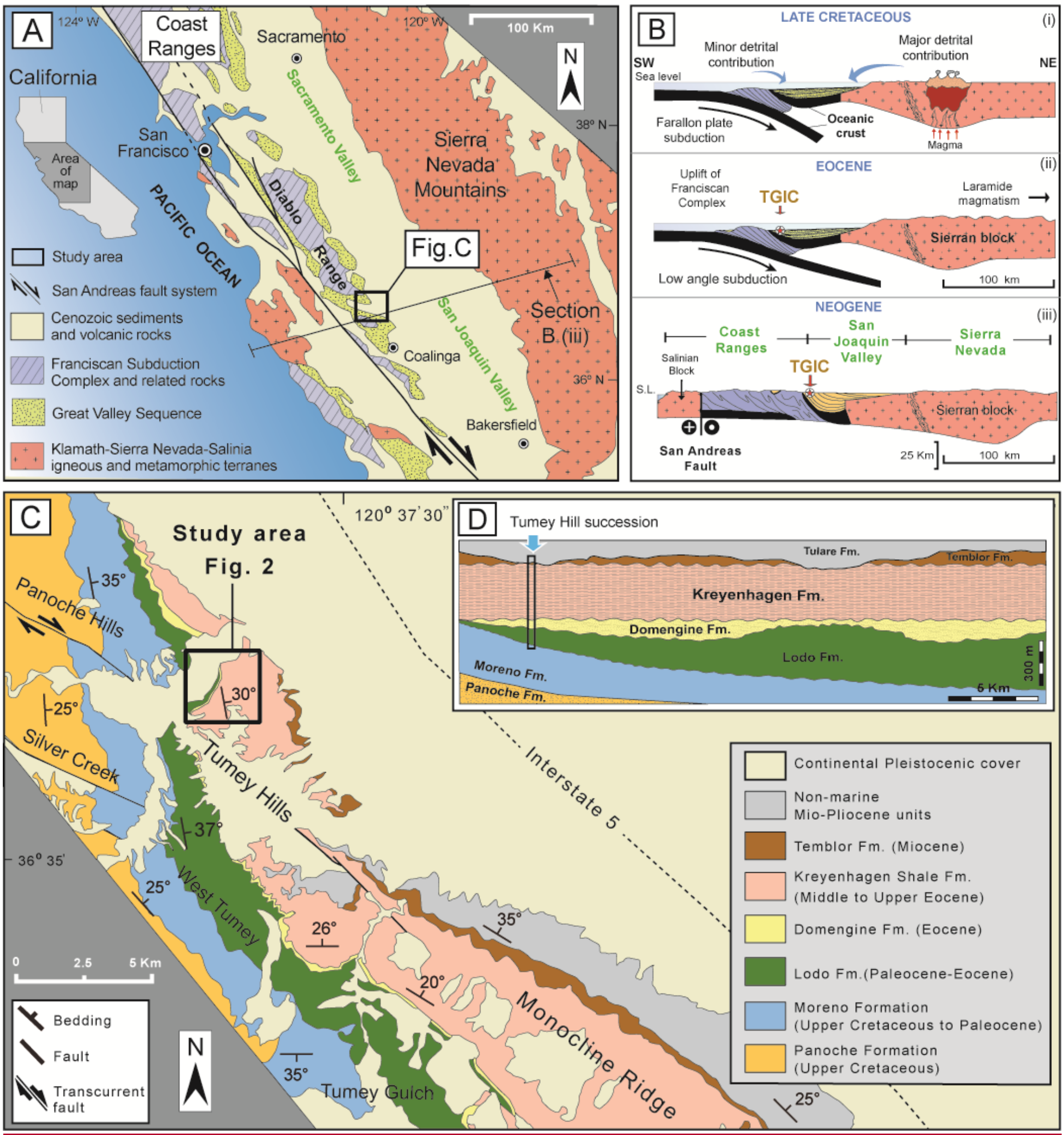
A
Coast Ranges
124° W
120° W
100 Km
California
Area of map
Sacramento
Sacramento Valley
San Francisco
Sierra Nevada Mountains
38° N
Diablo Range
PACIFIC OCEAN
Fig.C
Study area
San Andreas fault system
Cenozoic sediments and volcanic rocks
Franciscan Subduction Complex and related rocks
Great Valley Sequence
Klamath-Sierra Nevada-Salinia igneous and metamorphic terranes
Section B.(iii)
Coalinga
San Joaquin Valley
36° N
Bakersfield
B
LATE CRETACEOUS
(i)
SW
Sea level
Minor detrital contribution
Major detrital contribution
NE
Farallon plate subduction
Oceanic crust
Magma
EOCENE
(ii)
Uplift of Franciscan Complex
TGIC
Laramide magmatism
Sierran block
Low angle subduction
100 km
NEOGENE
(iii)
Coast Ranges
San Joaquin Valley
Sierra Nevada
Salinian Block
S.L.
TGIC
Sierran block
San Andreas Fault
25 Km
100 km
C
Study area
Fig. 2
120° 37' 30"
Panoche Hills
35°
30°
25°
Silver Creek
Tumey Hills
37°
36° 35'
25°
West Tumey
26°
35°
20°
Monocline Ridge
Interstate 5
0
2.5
5 Km
Bedding
Fault
Transcurrent fault
N
35°
Tumey Gulch
25°
D
Tumey Hill succession
Tulare Fm.
Temblor Fm.
Kreyenhagen Fm.
Domengine Fm.
Lodo Fm.
Moreno Fm.
Panoche Fm.
300 m
5 Km
Continental Pleistocenic cover
Non-marine Mio-Pliocene units
Temblor Fm. (Miocene)
Kreyenhagen Shale Fm. (Middle to Upper Eocene)
Domengine Fm. (Eocene)
Lodo Fm.(Paleocene-Eocene)
Moreno Formation (Upper Cretaceous to Paleocene)
Panoche Formation (Upper Cretaceous)

Fig. 2

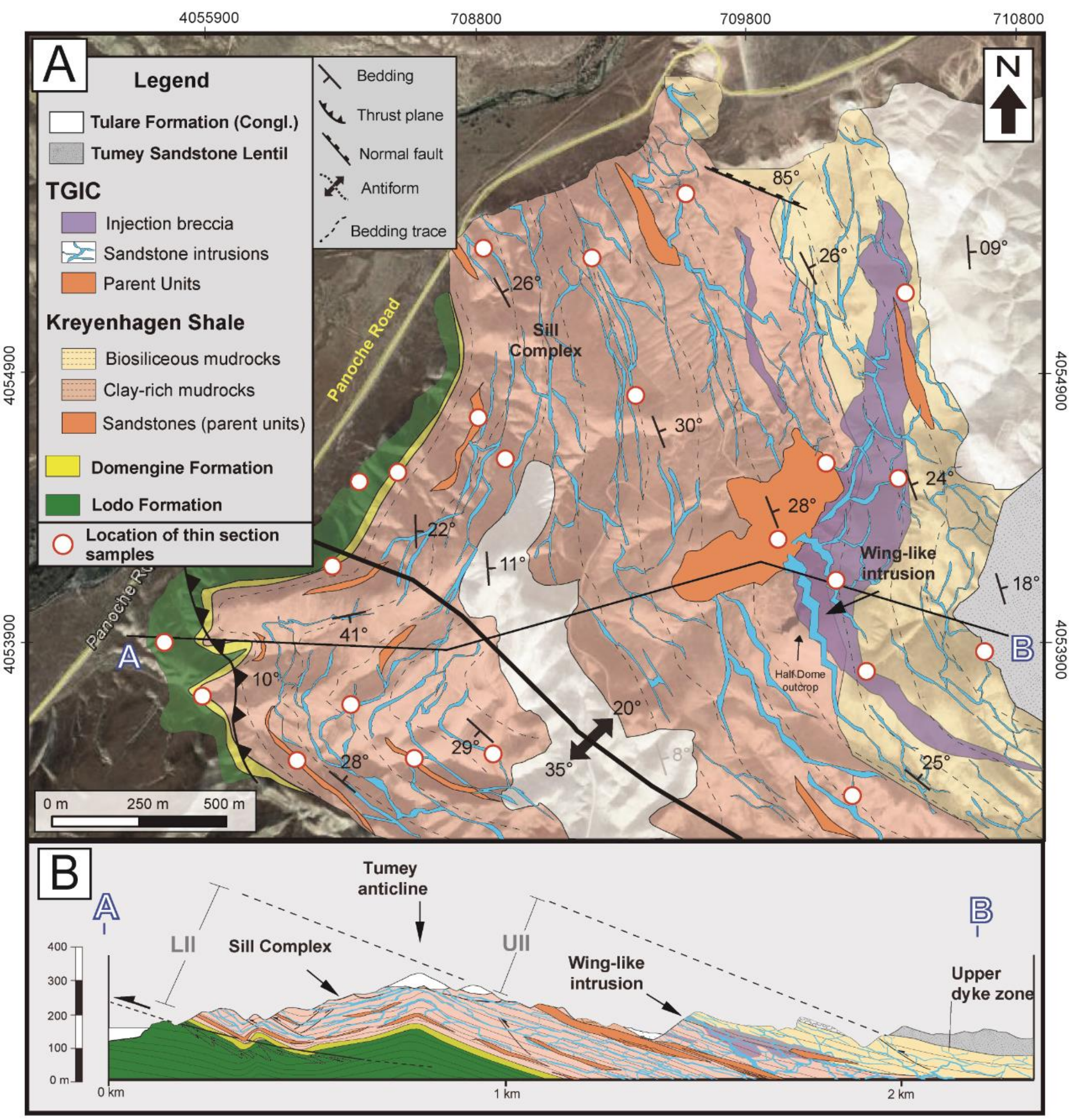

4055900
708800
709800
710800
4054900
4053900
A
Legend
Tulare Formation (Congl.)
Tumey Sandstone Lentil
TGIC
Injection breccia
Sandstone intrusions
Parent Units
Kreyenhagen Shale
Biosiliceous mudrocks
Clay-rich mudrocks
Sandstones (parent units)
Domengine Formation
Lodo Formation
Location of thin section samples
Bedding
Thrust plane
Normal fault
Antiform
Bedding trace
N
Panoche Road
Panoche Rd
Sill Complex
Wing-like intrusion
Half-Dome outcrop
85°
26°
09°
30°
28°
24°
22°
11°
18°
41°
10°
20°
29°
28°
35°
25°
0 m
250 m
500 m
B
A
B
Tumey anticline
LII
UII
Sill Complex
Wing-like intrusion
Upper dyke zone
400
300
200
100
0 m
0 km
1 km
2 km

Fig. 3

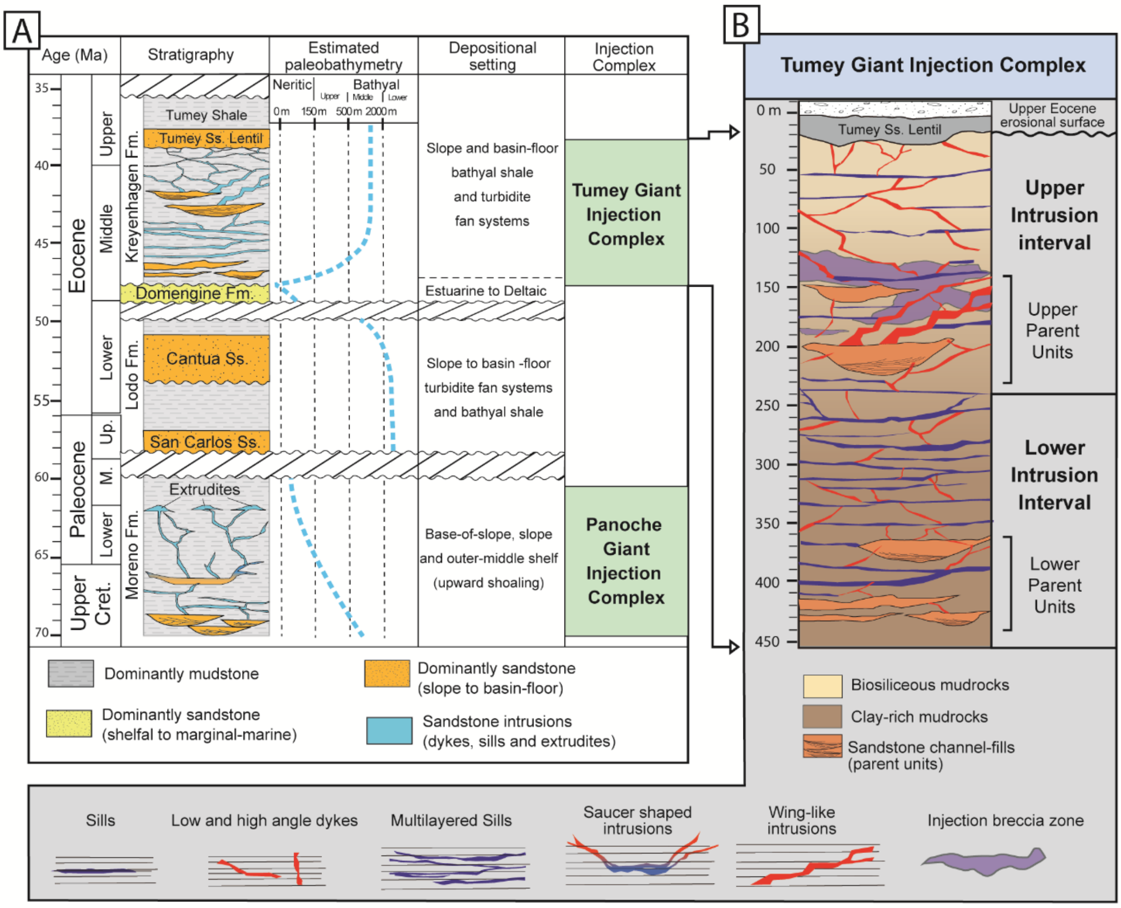
A
Age (Ma)
Stratigraphy
Estimated paleobathymetry
Depositional setting
Injection Complex
Neritic
Bathyal
Upper
Middle
Lower
0m
150m
500m
2000m
Eocene
Upper
Middle
Lower
Paleocene
Up.
M.
Lower
Upper Cret.
Kreyenhagen Fm.
Lodo Fm.
Moreno Fm.
Tumey Shale
Tumey Ss. Lentil
Domengine Fm.
Cantua Ss.
San Carlos Ss.
Extrudites
Slope and basin-floor bathyal shale and turbidite fan systems
Estuarine to Deltaic
Slope to basin -floor turbidite fan systems and bathyal shale
Base-of-slope, slope and outer-middle shelf (upward shoaling)
Tumey Giant Injection Complex
Panoche Giant Injection Complex
Dominantly mudstone
Dominantly sandstone (slope to basin-floor)
Dominantly sandstone (shelfal to marginal-marine)
Sandstone intrusions (dykes, sills and extrudites)
B
Tumey Giant Injection Complex
0 m
Tumey Ss. Lentil
Upper Eocene erosional surface
Upper Intrusion interval
Upper Parent Units
Lower Intrusion Interval
Lower Parent Units
Biosiliceous mudrocks
Clay-rich mudrocks
Sandstone channel-fills (parent units)
Sills
Low and high angle dykes
Multilayered Sills
Saucer shaped intrusions
Wing-like intrusions
Injection breccia zone

Fig. 4

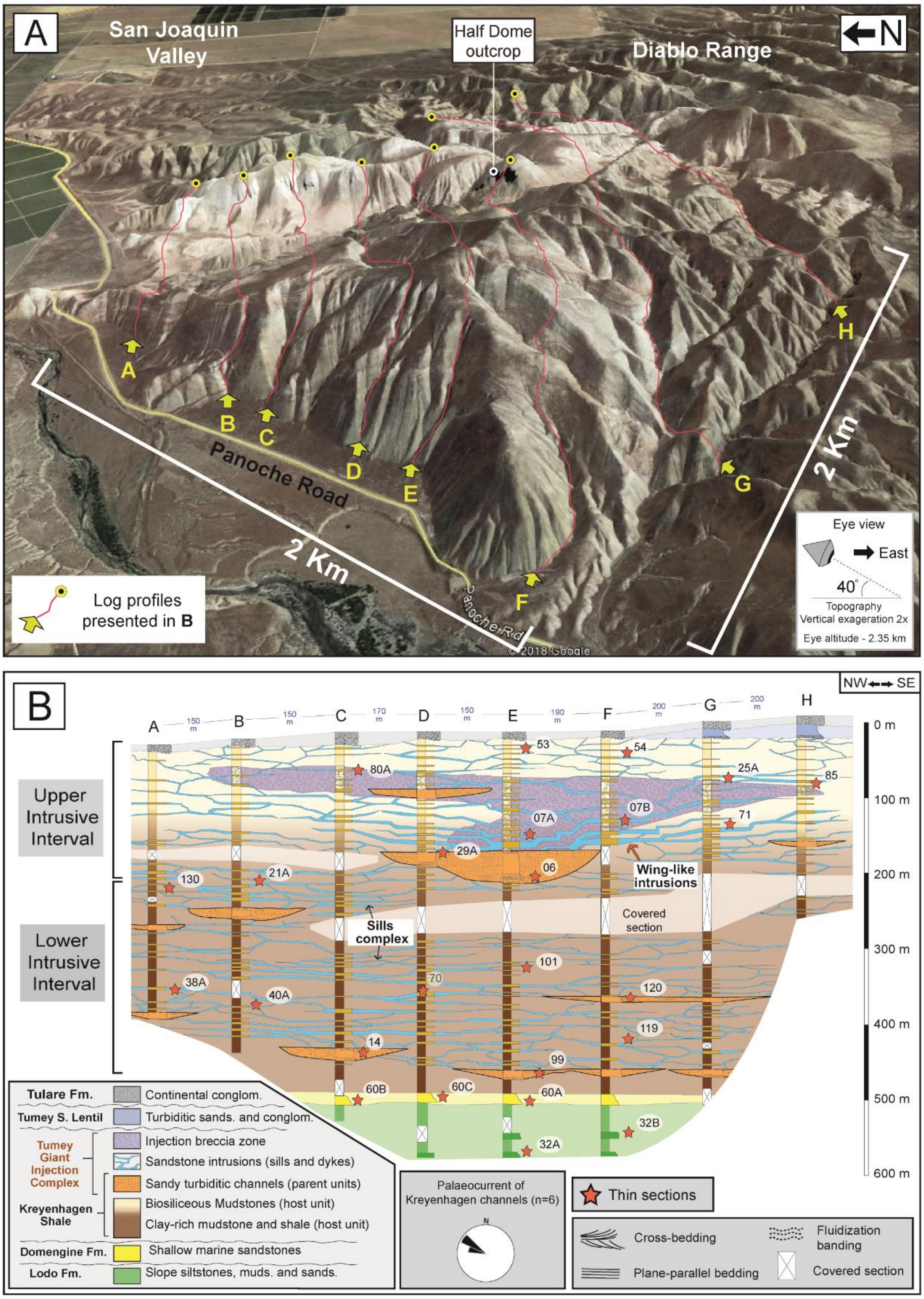

A
San Joaquin Valley
Half Dome outcrop
Diablo Range
N
A
B
C
D
E
F
G
H
Panoche Road
Panoche Rd
2 Km
2 Km
Eye view
East
40°
Topography Vertical exageration 2x
Eye altitude - 2.35 km
Log profiles presented in B
© 2018 Google
B
NW SE
A B C D E F G H
150 m
150 m
170 m
150 m
190 m
200 m
200 m
0 m
100 m
200 m
300 m
400 m
500 m
600 m
Upper Intrusive Interval
Lower Intrusive Interval
80A
53
54
25A
85
07B
07A
71
29A
06
Wing-like intrusions
130
21A
Sills complex
Covered section
101
38A
40A
70
120
119
14
99
60B
60C
60A
32B
32A
Tulare Fm.
Continental conglom.
Tumey S. Lentil
Turbiditic sands. and conglom.
Tumey Giant Injection Complex
Injection breccia zone
Sandstone intrusions (sills and dykes)
Sandy turbiditic channels (parent units)
Kreyenhagen Shale
Biosiliceous Mudstones (host unit)
Clay-rich mudstone and shale (host unit)
Domengine Fm.
Shallow marine sandstones
Lodo Fm.
Slope siltstones, muds. and sands.
Palaeocurrent of Kreyenhagen channels (n=6)
N
Thin sections
Cross-bedding
Fluidization banding
Plane-parallel bedding
Covered section

Fig. 5

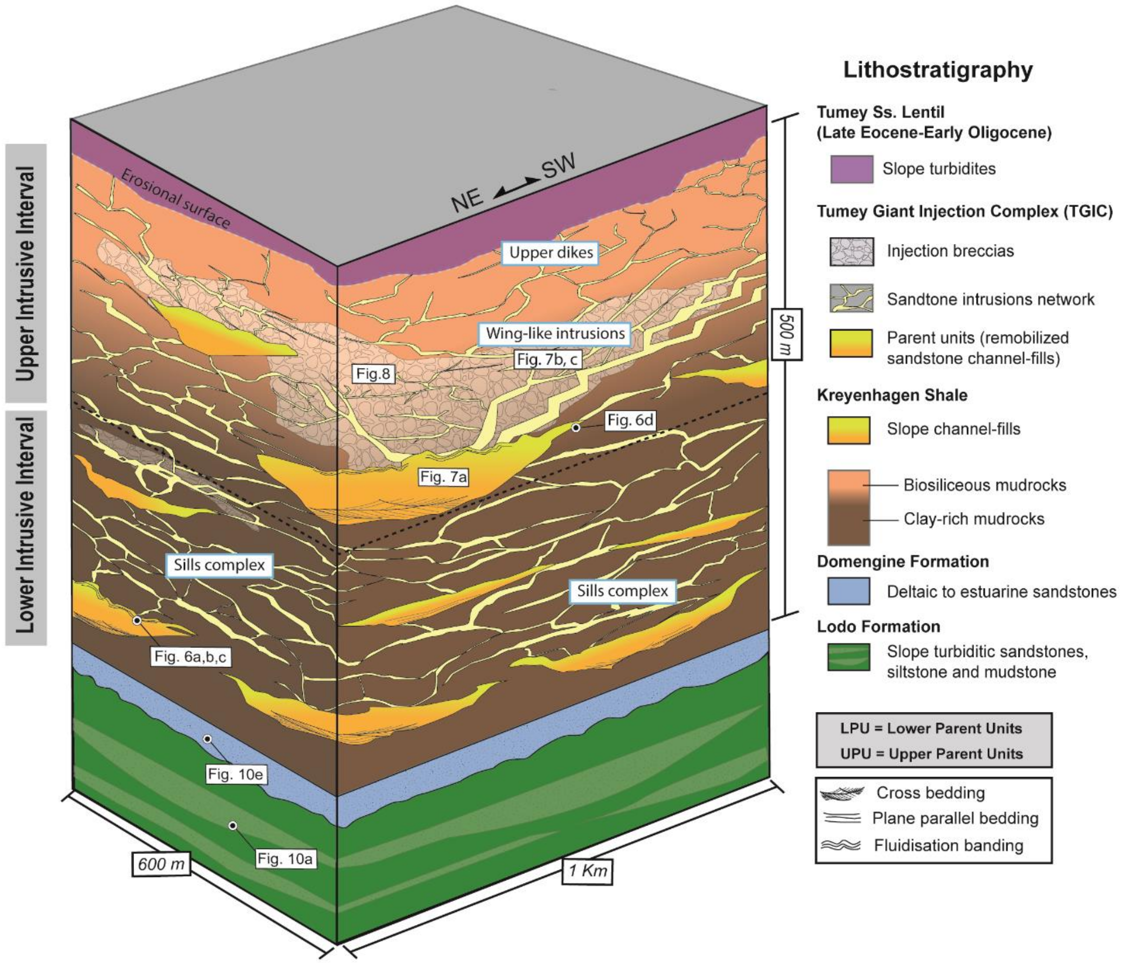

Upper Intrusive Interval
Lower Intrusive Interval
Erosional surface
NE
SW
Upper dikes
Wing-like intrusions
Fig. 7b, c
Fig.8
Fig. 6d
Fig. 7a
Sills complex
Sills complex
Fig. 6a,b,c
Fig. 10e
Fig. 10a
600 m
1 Km
500 m
Lithostratigraphy
Tumey Ss. Lentil
(Late Eocene-Early Oligocene)
Slope turbidites
Tumey Giant Injection Complex (TGIC)
Injection breccias
Sandtone intrusions network
Parent units (remobilized sandstone channel-fills)
Kreyenhagen Shale
Slope channel-fills
Biosiliceous mudrocks
Clay-rich mudrocks
Domengine Formation
Deltaic to estuarine sandstones
Lodo Formation
Slope turbiditic sandstones, siltstone and mudstone
LPU = Lower Parent Units
UPU = Upper Parent Units
Cross bedding
Plane parallel bedding
Fluidisation banding

Fig. 6

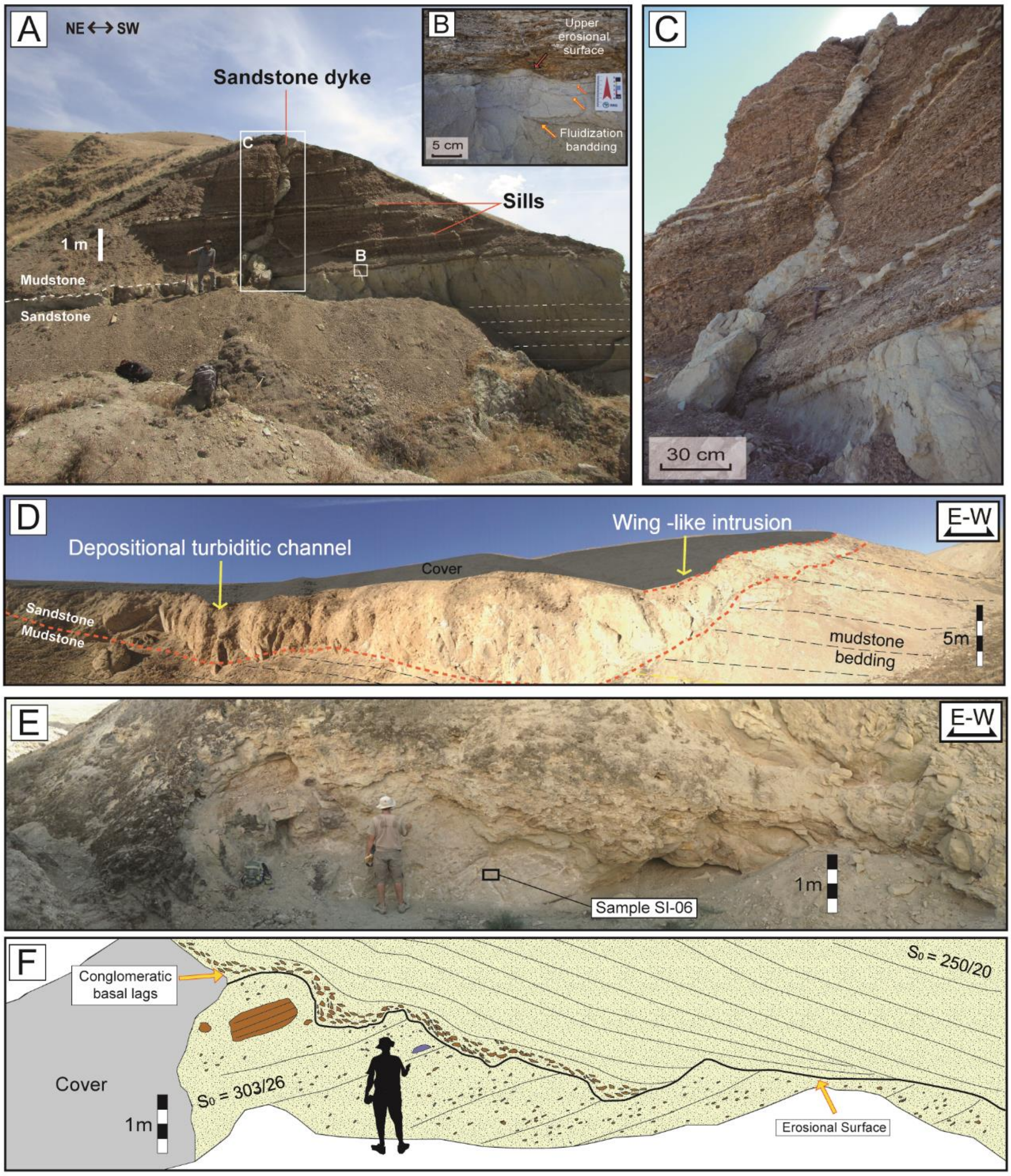
A
NE ↔ SW
Sandstone dyke
C
B
Sills
1 m
Mudstone
Sandstone
Upper erosional surface
Fluidization banding
5 cm
30 cm
D
Depositional turbiditic channel
Cover
Wing -like intrusion
E-W
Sandstone
Mudstone
mudstone bedding
5m
E
E-W
1m
Sample SI-06
F
Conglomeratic basal lags
S0 = 250/20
Cover
1m
S0 = 303/26
Erosional Surface

Fig. 7

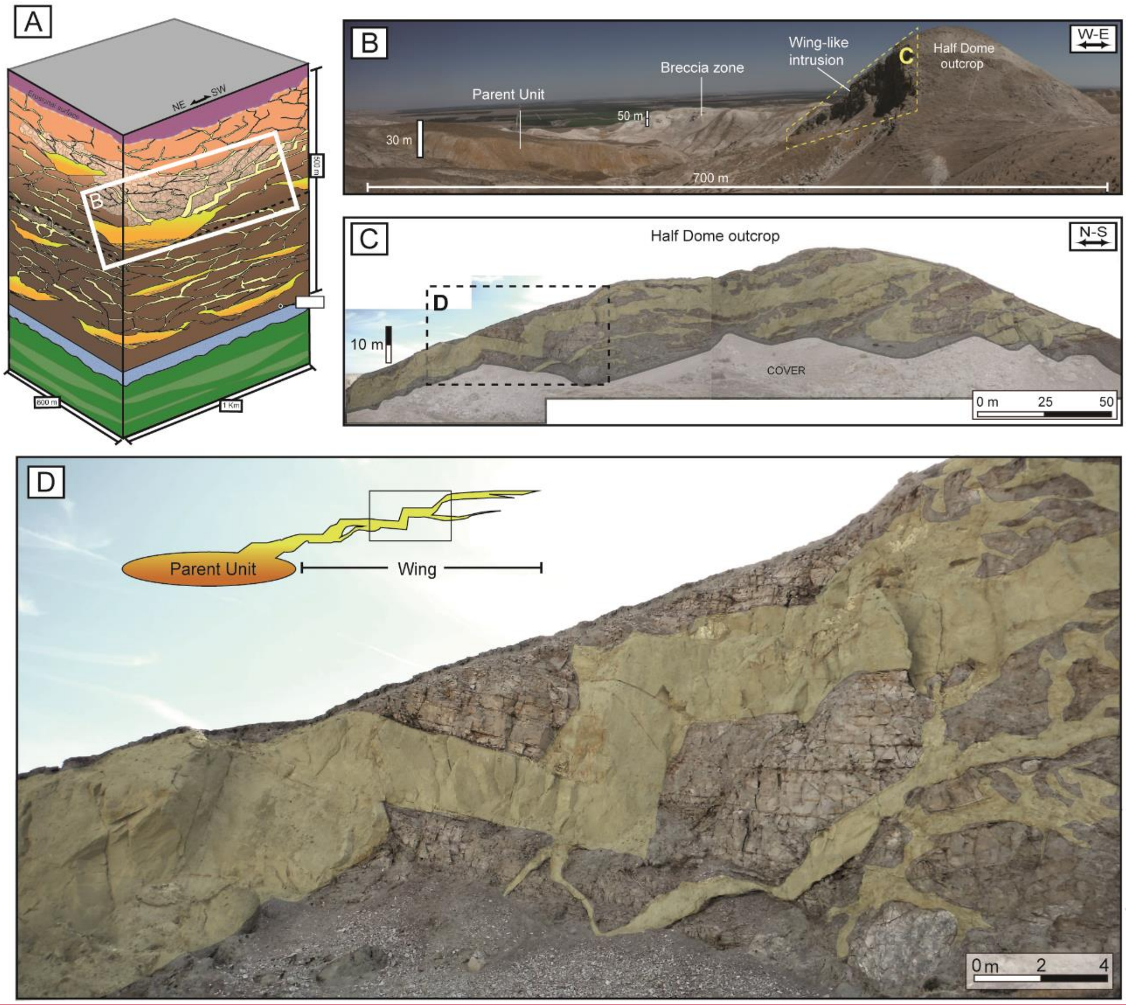
A
NE
SW
B
Parent Unit
Breccia zone
Wing-like
intrusion
C
Half Dome
outcrop
W-E
30 m
50 m
700 m
C
Half Dome outcrop
N-S
D
10 m
COVER
0 m
25
50
D
Parent Unit
Wing
0 m
2
4

Fig. 8

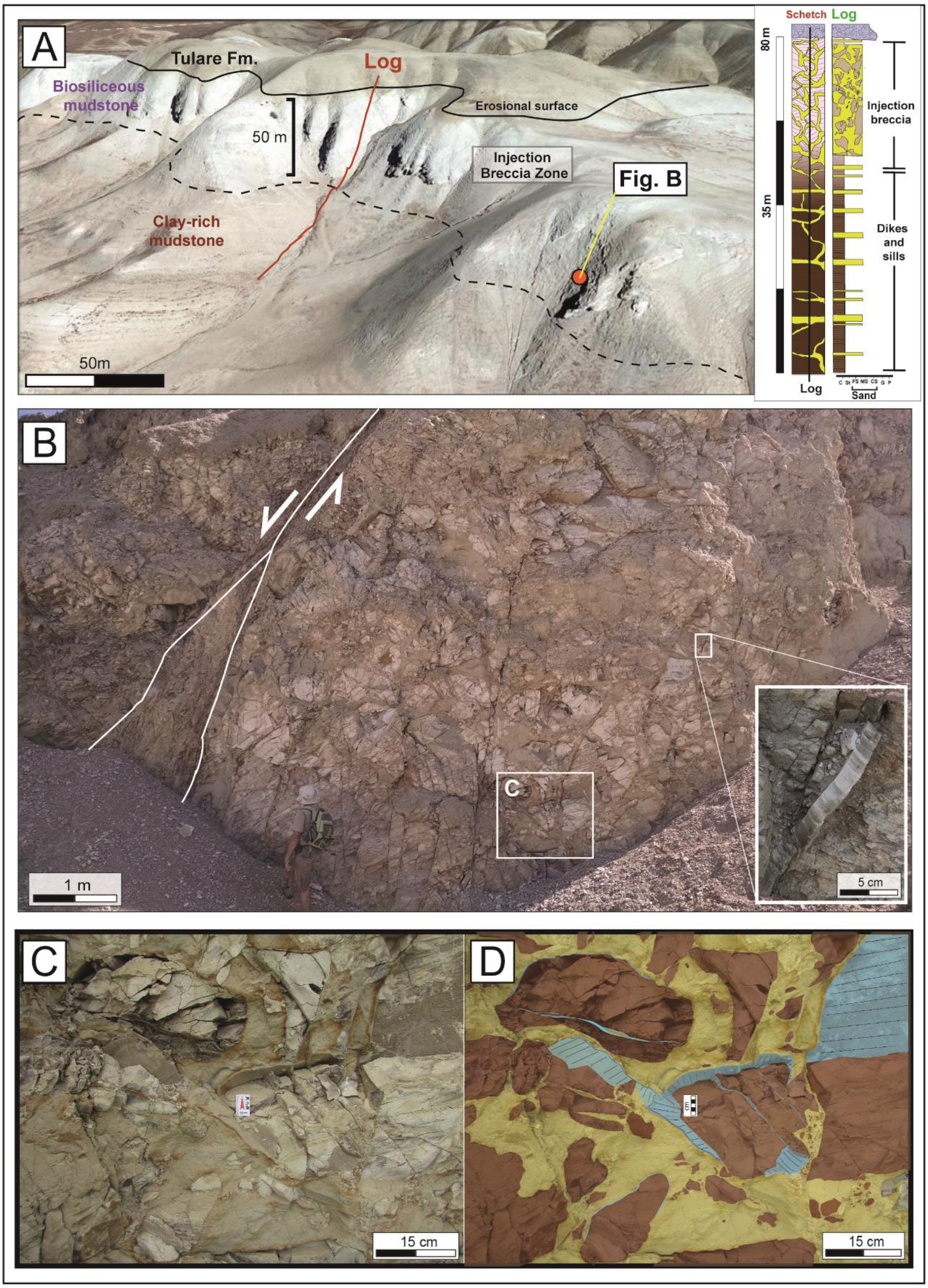
A
Tulare Fm.
Log
Biosiliceous mudstone
50 m
Erosional surface
Injection Breccia Zone
Fig. B
Clay-rich mudstone
50m
Schetch
Log
80 m
35 m
Injection breccia
Dikes and sills
Log
Sand
B
C
1 m
5 cm
C
15 cm
D
15 cm

Fig. 9

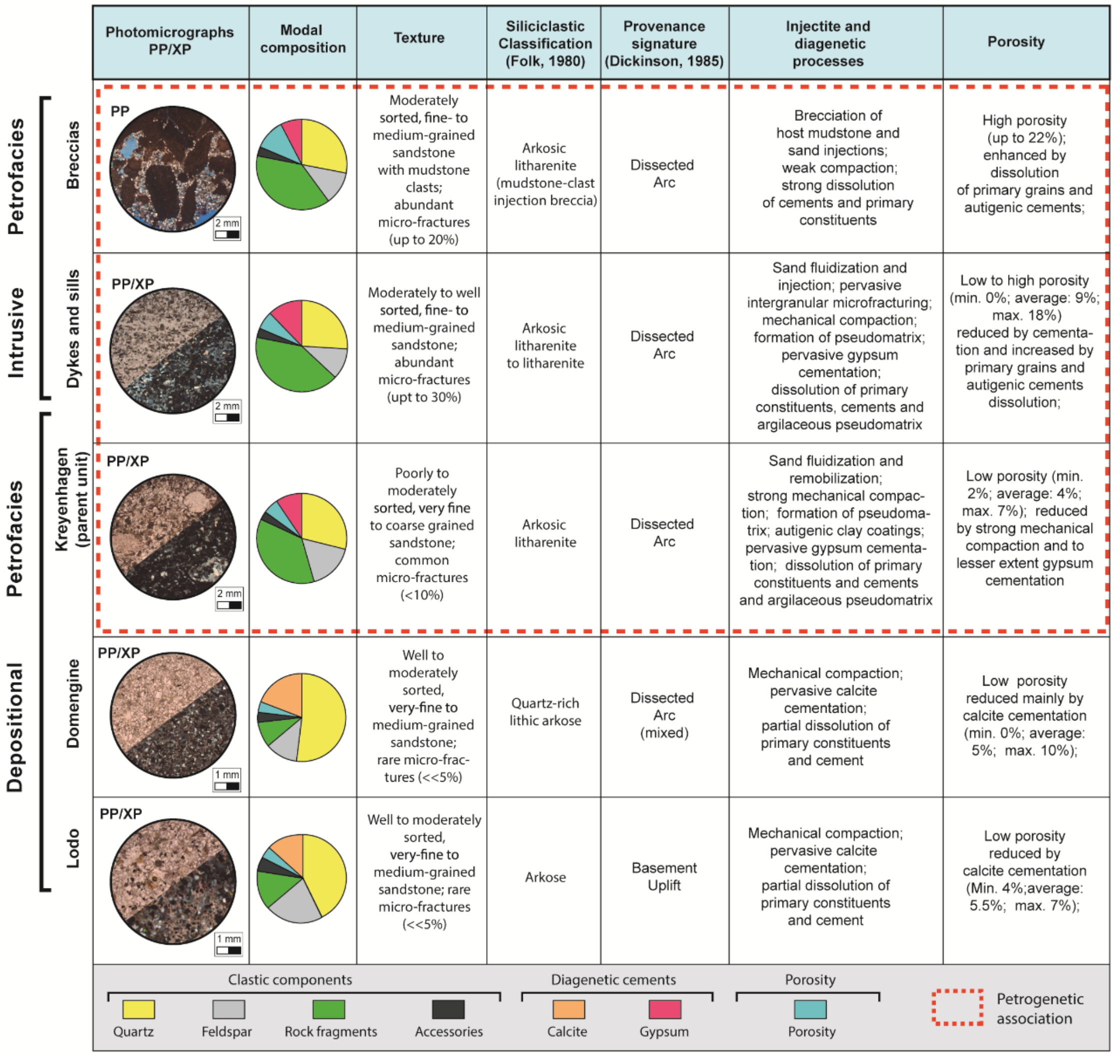
Photomicrographs PP/XP
Modal composition
Texture
Siliciclastic Classification (Folk, 1980)
Provenance signature (Dickinson, 1985)
Injectite and diagenetic processes
Porosity
Intrusive Petrofacies
Breccias
PP
2 mm
Moderately sorted, fine- to medium-grained sandstone with mudstone clasts; abundant micro-fractures (up to 20%)
Arkosic litharenite (mudstone-clast injection breccia)
Dissected Arc
Brecciation of host mudstone and sand injections; weak compaction; strong dissolution of cements and primary constituents
High porosity (up to 22%); enhanced by dissolution of primary grains and autigenic cements;
Dykes and sills
PP/XP
2 mm
Moderately to well sorted, fine- to medium-grained sandstone; abundant micro-fractures (upt to 30%)
Arkosic litharenite to litharenite
Dissected Arc
Sand fluidization and injection; pervasive intergranular microfracturing; mechanical compaction; formation of pseudomatrix; pervasive gypsum cementation; dissolution of primary constituents, cements and argilaceous pseudomatrix
Low to high porosity (min. 0%; average: 9%; max. 18%) reduced by cementation and increased by primary grains and autigenic cements dissolution;
Depositional Petrofacies
Kreyenhagen (parent unit)
PP/XP
2 mm
Poorly to moderately sorted, very fine to coarse grained sandstone; common micro-fractures (<10%)
Arkosic litharenite
Dissected Arc
Sand fluidization and remobilization; strong mechanical compaction; formation of pseudomatrix; autigenic clay coatings; pervasive gypsum cementation; dissolution of primary constituents and cements and argilaceous pseudomatrix
Low porosity (min. 2%; average: 4%; max. 7%); reduced by strong mechanical compaction and to lesser extent gypsum cementation
Domengine
PP/XP
1 mm
Well to moderately sorted, very-fine to medium-grained sandstone; rare micro-fractures (<<5%)
Quartz-rich lithic arkose
Dissected Arc (mixed)
Mechanical compaction; pervasive calcite cementation; partial dissolution of primary constituents and cement
Low porosity reduced mainly by calcite cementation (min. 0%; average: 5%; max. 10%);
Lodo
PP/XP
1 mm
Well to moderately sorted, very-fine to medium-grained sandstone; rare micro-fractures (<<5%)
Arkose
Basement Uplift
Mechanical compaction; pervasive calcite cementation; partial dissolution of primary constituents and cement
Low porosity reduced by calcite cementation (Min. 4%;average: 5.5%; max. 7%);
Clastic components
Quartz
Feldspar
Rock fragments
Accessories
Diagenetic cements
Calcite
Gypsum
Porosity
Porosity
Petrogenetic association

Fig. 10

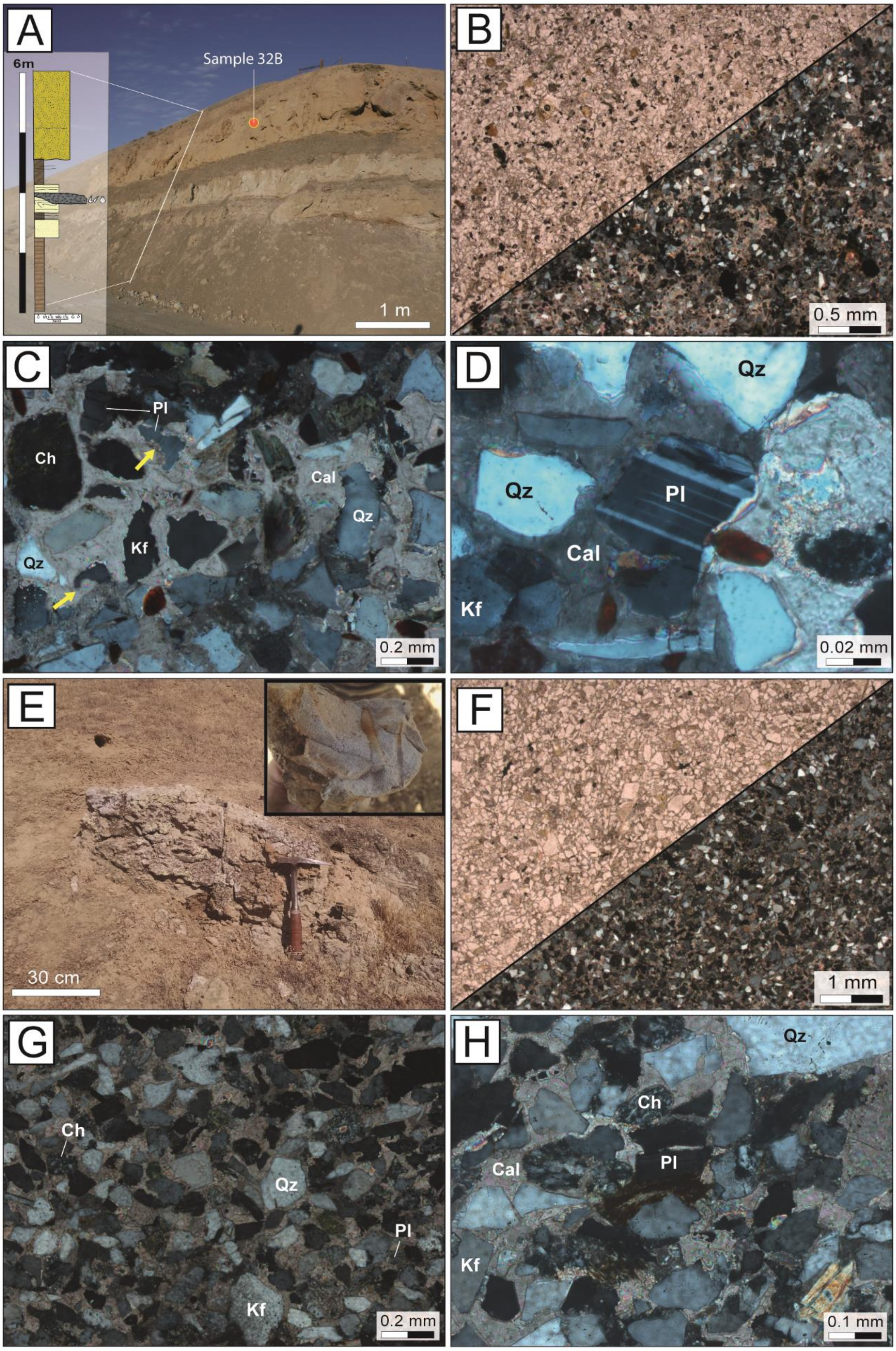
A
6m
Sample 32B
1 m
B
0.5 mm
C
Pl
Ch
Cal
Qz
Kf
Qz
0.2 mm
D
Qz
Qz
Pl
Cal
Kf
0.02 mm
E
30 cm
F
1 mm
G
Ch
Qz
Pl
Kf
0.2 mm
H
Qz
Ch
Cal
Pl
Kf
0.1 mm

Fig. 11

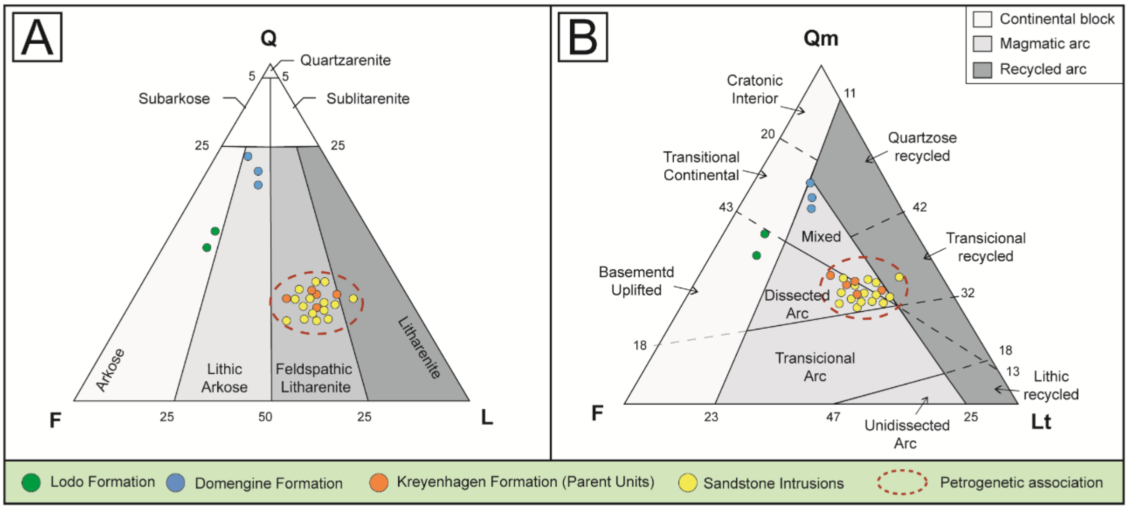
A
Q
Quartzarenite
5
5
Subarkose
Sublitarenite
25
25
Arkose
Lithic
Arkose
Feldspathic
Litharenite
Litharenite
F
25
50
25
L
B
Qm
Continental block
Magmatic arc
Recycled arc
Cratonic
Interior
11
20
Quartzose
recycled
Transitional
Continental
43
42
Mixed
Transicional
recycled
Basementd
Uplifted
Dissected
Arc
32
18
18
Transicional
Arc
13
Lithic
recycled
F
23
47
Unidissected
Arc
25
Lt
Lodo Formation
Domengine Formation
Kreyenhagen Formation (Parent Units)
Sandstone Intrusions
Petrogenetic association

Fig. 12

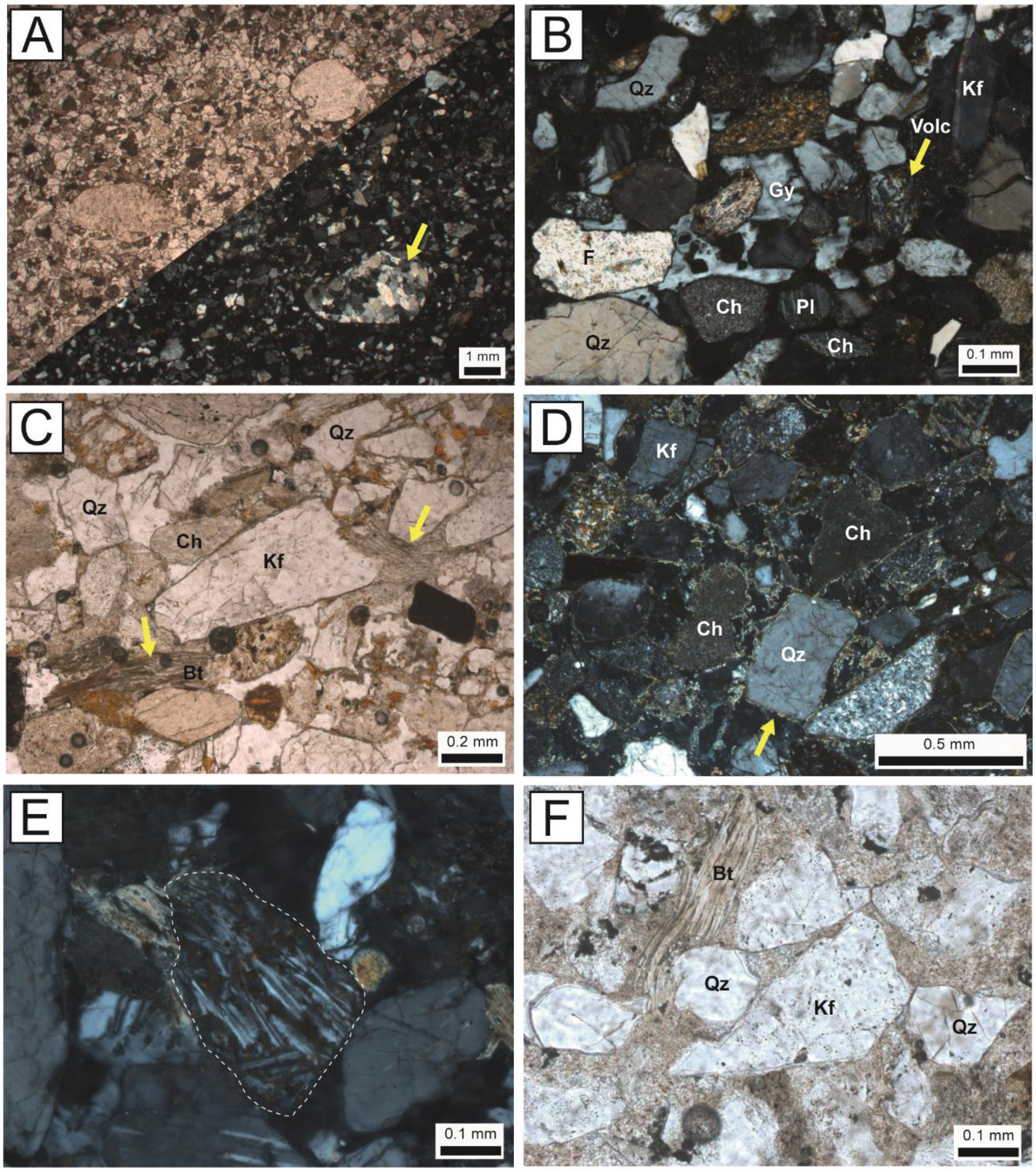
A
1 mm
B
Qz
Kf
Volc
Gy
F
Ch
Pl
Qz
Ch
0.1 mm
C
Qz
Qz
Ch
Kf
Bt
0.2 mm
D
Kf
Ch
Ch
Qz
0.5 mm
E
0.1 mm
F
Bt
Qz
Kf
Qz
0.1 mm

Fig. 13

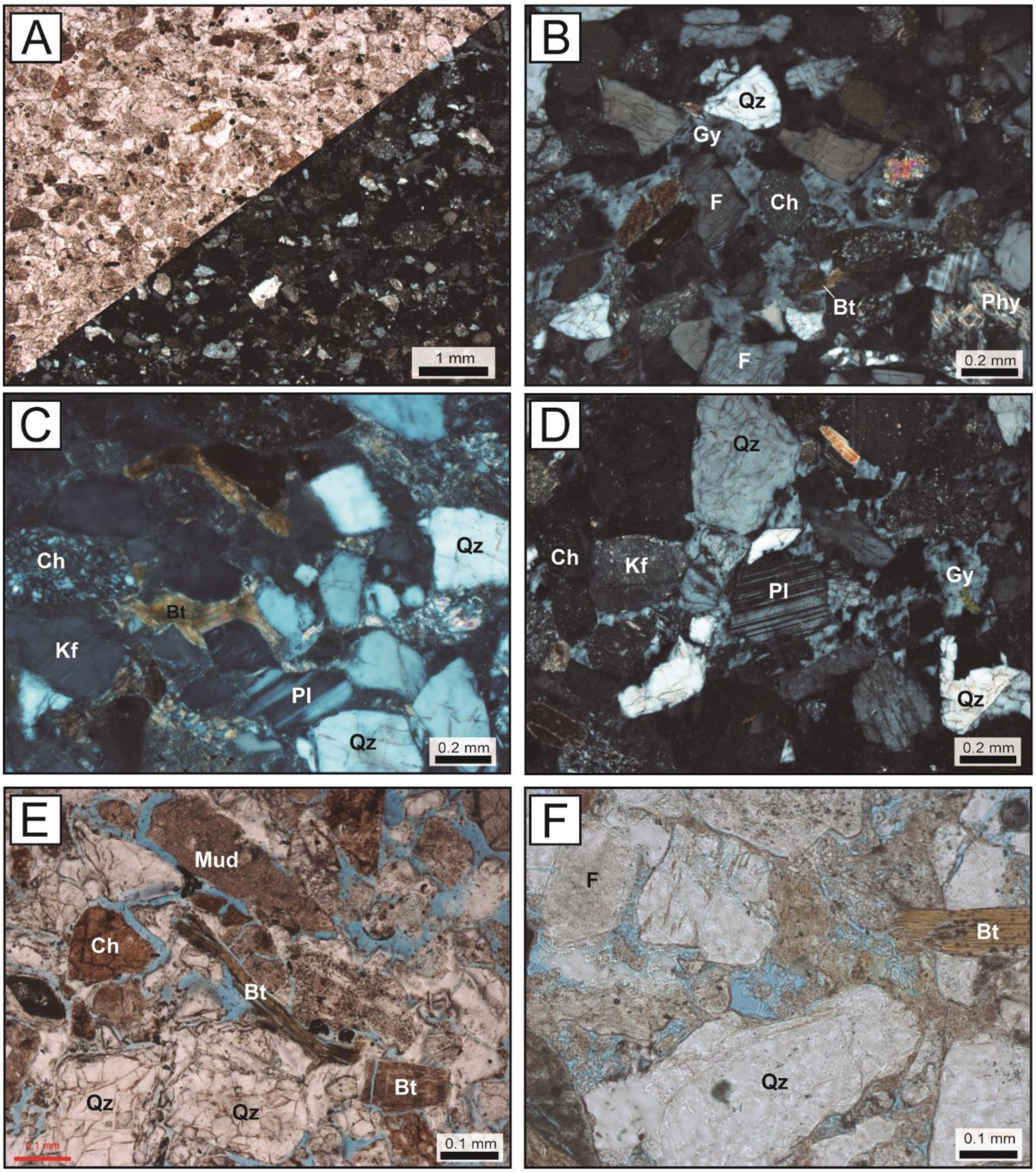
A
1 mm
B
Qz
Gy
F
Ch
Bt
Phy
F
0.2 mm
C
Ch
Qz
Bt
Kf
Pl
Qz
0.2 mm
D
Qz
Ch
Kf
Pl
Gy
Qz
0.2 mm
E
Mud
Ch
Bt
Bt
Qz
Qz
0.1 mm
F
F
Bt
Qz
0.1 mm

Fig. 14

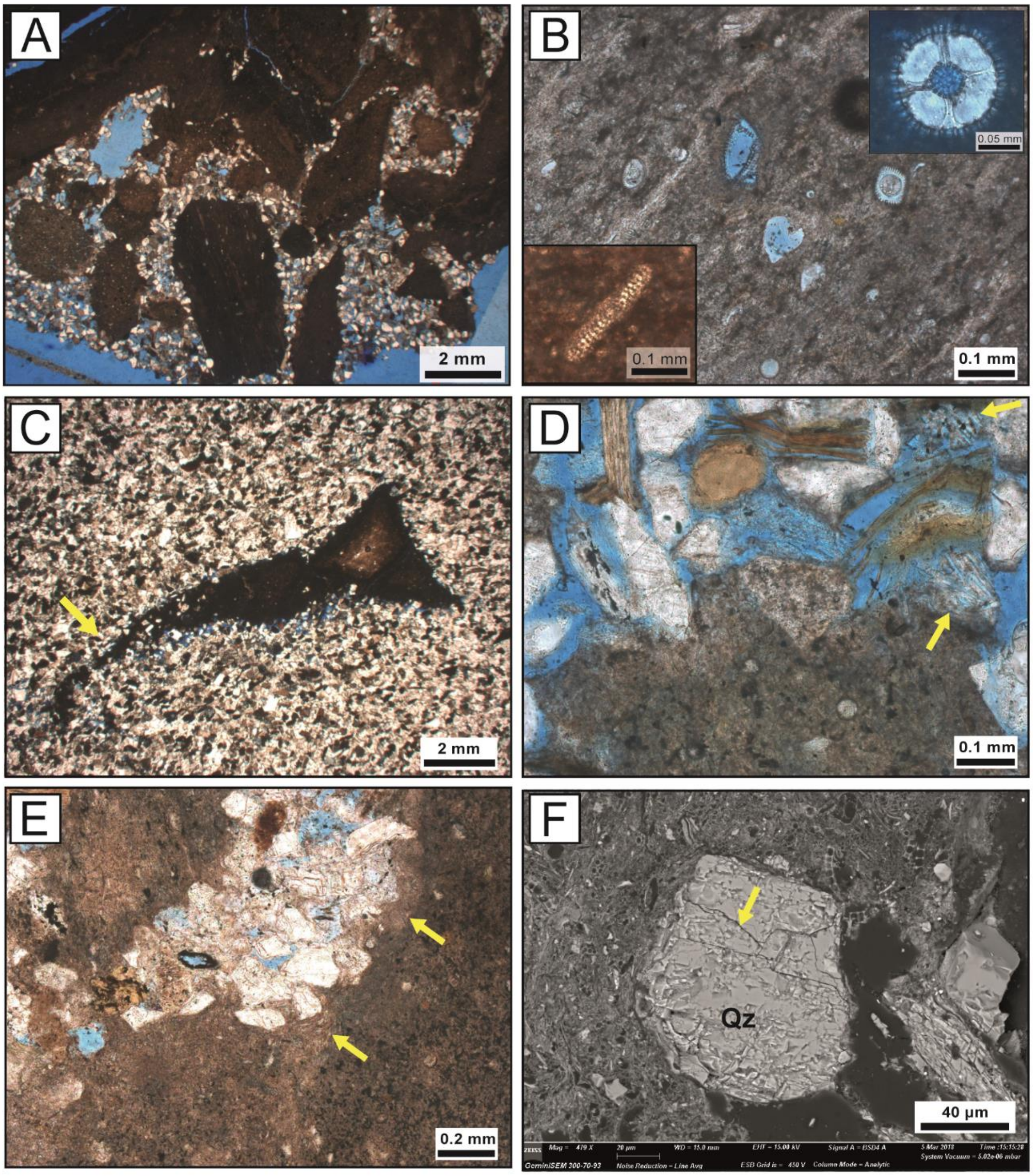

Fig.15

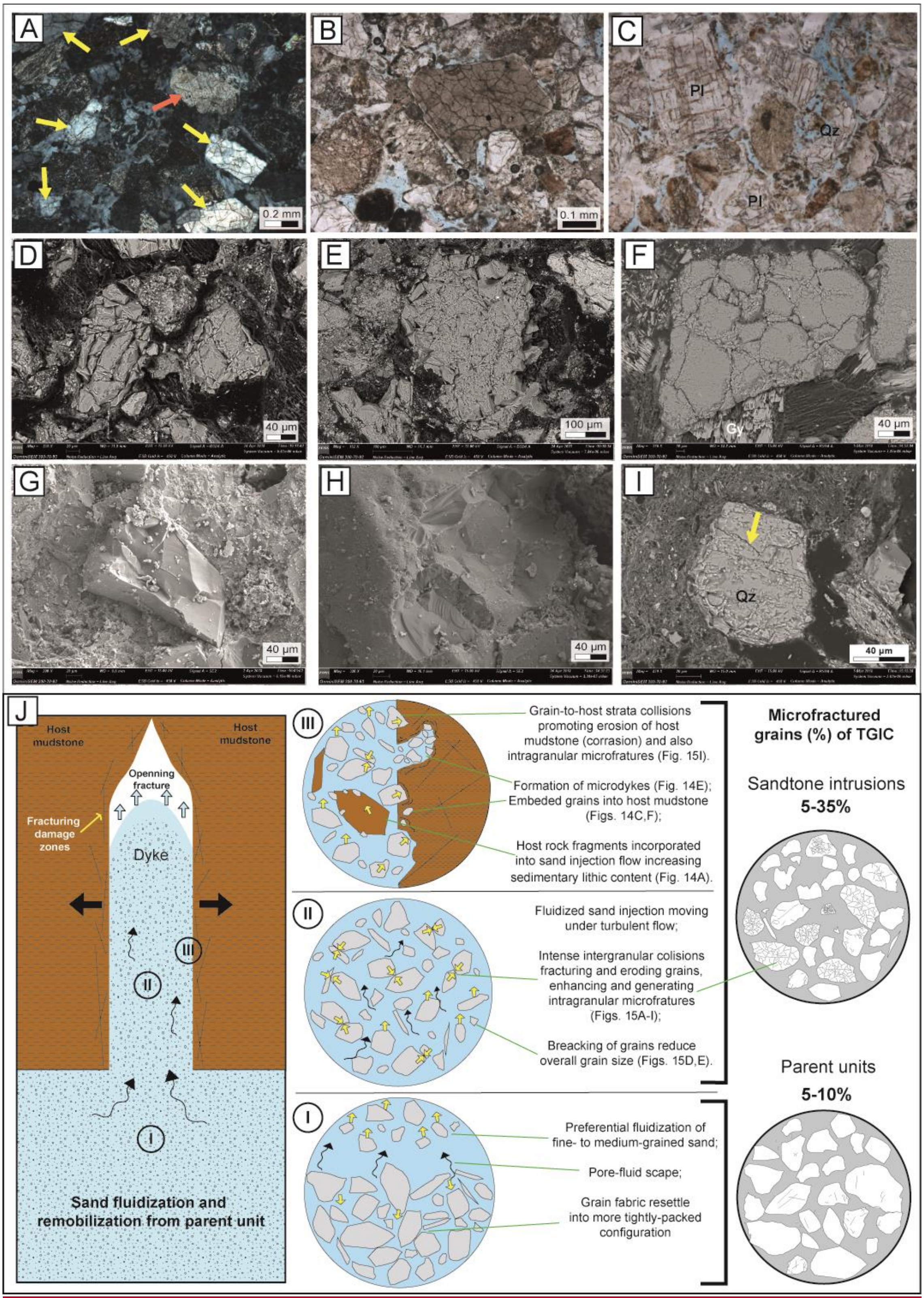
A
0.2 mm
B
0.1 mm
C
Pl
Qz
Pl
D
40 µm
E
100 µm
F
Gy
40 µm
G
40 µm
H
40 µm
I
Qz
40 µm
J
Host mudstone
Host mudstone
Openning fracture
Fracturing damage zones
Dyke
Sand fluidization and remobilization from parent unit
III
Grain-to-host strata collisions promoting erosion of host mudstone (corrasion) and also intragranular microfratures (Fig. 15I).
Formation of microdykes (Fig. 14E);
Embeded grains into host mudstone (Figs. 14C,F);
Host rock fragments incorporated into sand injection flow increasing sedimentary lithic content (Fig. 14A).
II
Fluidized sand injection moving under turbulent flow;
Intense intergranular colisions fracturing and eroding grains, enhancing and generating intragranular microfratures (Figs. 15A-I);
Breacking of grains reduce overall grain size (Figs. 15D,E).
I
Preferential fluidization of fine- to medium-grained sand;
Pore-fluid scape;
Grain fabric resettle into more tightly-packed configuration
Microfractured grains (%) of TGIC
Sandtone intrusions
5-35%
Parent units
5-10%

Fig. 16

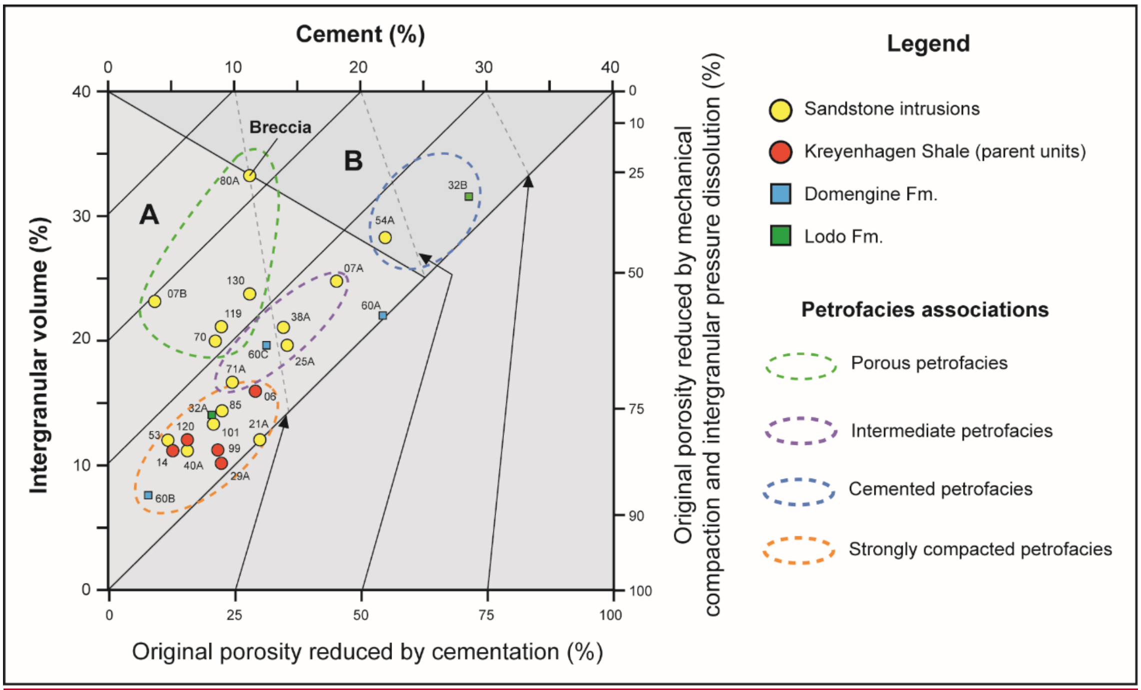

Cement (%)
Intergranular volume (%)
Original porosity reduced by cementation (%)
Original porosity reduced by mechanical compaction and intergranular pressure dissolution (%)
Breccia
A
B
Legend
Sandstone intrusions
Kreyenhagen Shale (parent units)
Domengine Fm.
Lodo Fm.
Petrofacies associations
Porous petrofacies
Intermediate petrofacies
Cemented petrofacies
Strongly compacted petrofacies

Fig. 17

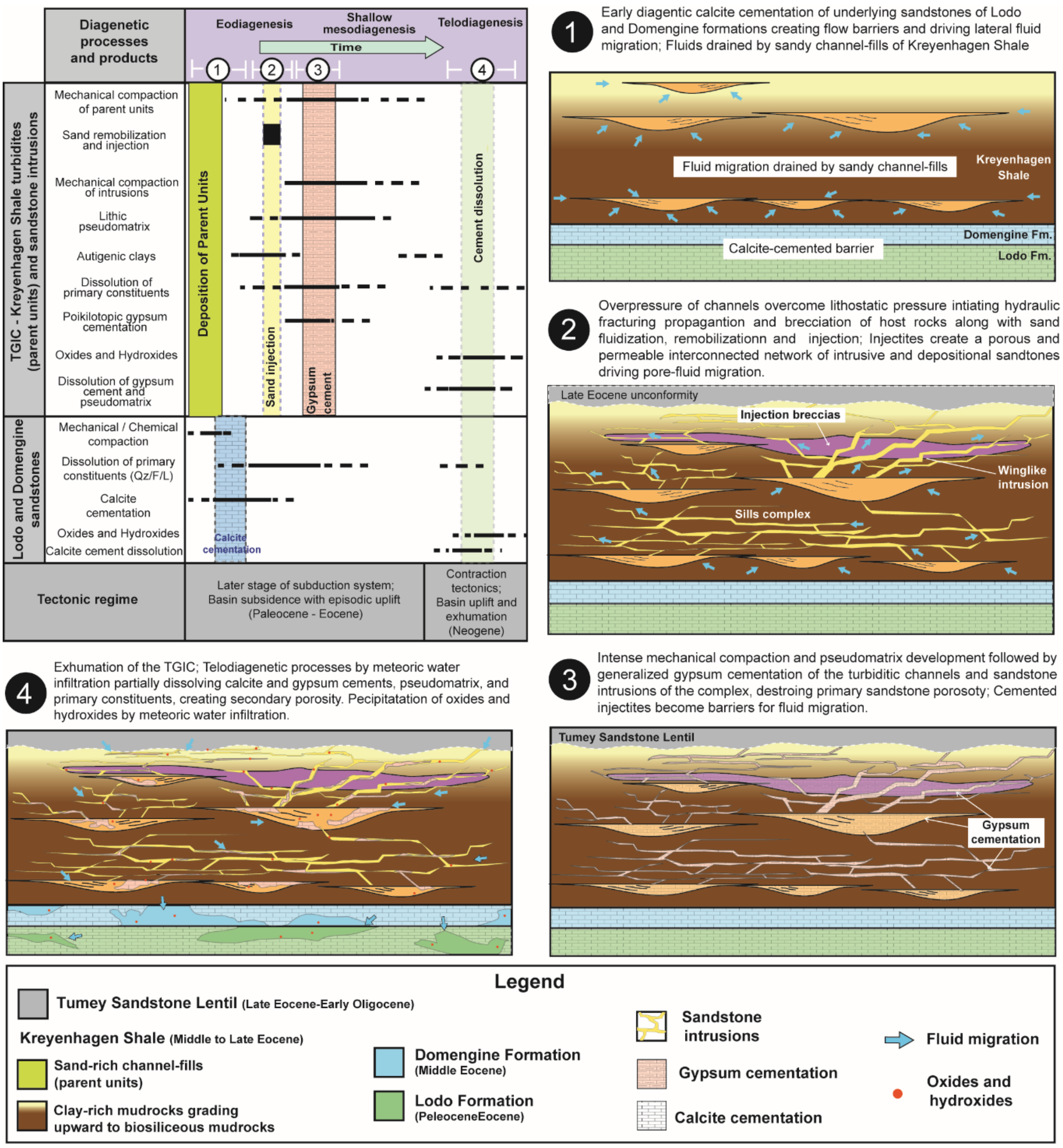

Diagenetic processes and products
Eodiagenesis
Shallow mesodiagenesis
Telodiagenesis
Time
1
2
3
4
TGIC - Kreyenhagen Shale turbidites (parent units) and sandstone intrusions
Mechanical compaction of parent units
Sand remobilization and injection
Mechanical compaction of intrusions
Lithic pseudomatrix
Autigenic clays
Dissolution of primary constituents
Poikilotopic gypsum cementation
Oxides and Hydroxides
Dissolution of gypsum cement and pseudomatrix
Deposition of Parent Units
Sand injection
Gypsum cement
Cement dissolution
Lodo and Domengine sandstones
Mechanical / Chemical compaction
Dissolution of primary constituents (Qz/F/L)
Calcite cementation
Oxides and Hydroxides
Calcite cement dissolution
Calcite cementation
Tectonic regime
Later stage of subduction system; Basin subsidence with episodic uplift (Paleocene - Eocene)
Contraction tectonics; Basin uplift and exhumation (Neogene)
1
Early diagentic calcite cementation of underlying sandstones of Lodo and Domengine formations creating flow barriers and driving lateral fluid migration; Fluids drained by sandy channel-fills of Kreyenhagen Shale
Fluid migration drained by sandy channel-fills
Kreyenhagen Shale
Domengine Fm.
Calcite-cemented barrier
Lodo Fm.
2
Overpressure of channels overcome lithostatic pressure intiating hydraulic fracturing propagantion and brecciation of host rocks along with sand fluidization, remobilizationn and injection; Injectites create a porous and permeable interconnected network of intrusive and depositional sandtones driving pore-fluid migration.
Late Eocene unconformity
Injection breccias
Winglike intrusion
Sills complex
4
Exhumation of the TGIC; Telodiagenetic processes by meteoric water infiltration partially dissolving calcite and gypsum cements, pseudomatrix, and primary constituents, creating secondary porosity. Pecipitatation of oxides and hydroxides by meteoric water infiltration.
3
Intense mechanical compaction and pseudomatrix development followed by generalized gypsum cementation of the turbiditic channels and sandstone intrusions of the complex, destroying primary sandstone porosity; Cemented injectites become barriers for fluid migration.
Tumey Sandstone Lentil
Gypsum cementation
Legend
Tumey Sandstone Lentil (Late Eocene-Early Oligocene)
Kreyenhagen Shale (Middle to Late Eocene)
Sand-rich channel-fills (parent units)
Clay-rich mudrocks grading upward to biosiliceous mudrocks
Domengine Formation (Middle Eocene)
Lodo Formation (PeleoceneEocene)
Sandstone intrusions
Gypsum cementation
Calcite cementation
Fluid migration
Oxides and hydroxides